https://doi.org/10.1016/j.ejmech.2022.114360

Design and synthesis of quinolinium-based derivatives targeting FtsZ for antibacterial evaluation and mechanistic study

Dong-Xiao Zhong [a], Meng-Ting She [a], Xiao-Chun Guo [a], Bo-Xin Zheng [a], Xuan-He Huang [a], Yi-Han Zhang [a], Hooi-Leng Ser [a], Wing-Leung Wong*[,b], Ning Sun*[,b,c], Yu-Jing Lu*[,a,d,e],

[a] School of Biomedical and Pharmaceutical Sciences, Guangdong University of Technology, Guangzhou 510006, P. R. China.

[b] The State Key Laboratory of Chemical Biology and Drug Discovery, Department of Applied Biology and Chemical Technology, The Hong Kong Polytechnic University, Hung Hom, Kowloon, Hong Kong, P. R. China.

[c] Guangzhou First People's Hospital, School of Medicine, South China University of Technology, Guangzhou 510180, P. R. China.

[d] Engineering Research Academy of High Value Utilization of Green Plants, Meizhou 514021, P. R. China.

[e] Golden Health (Guangdong) Biotechnology Co., Ltd, Foshan 528225, P. R. China.

* Corresponding author

Dr. Wing-Leung Wong Email: wing.leung.wong@polyu.edu.hk

Dr. Ning SUN Email: ning.sun@connect.polyu.hk

Dr. Yu-Jing LU Email: luyj@gdut.edu.cn

Abstract

The discovery of small molecular inhibitors targeting essential and conserved bacterial drug targets such as FtsZ protein is a promising approach to fight against multi-drug resistant bacteria. In the present study, two new series of FtsZ inhibitors based on a 1-methylquinolinium scaffold were synthesized. The inhibitors possess a variety of substituent groups including the cyclic or linear amine skeleton at the 2- and 4-position of the quinolinium ring for structure-activity relationship study. In general, the inhibitors bearing a cyclic amine substituent at the 4-position of the quinolinium ring showed better antibacterial activity (MIC down to 0.25 μg/mL) than that at the 2-position, especially against Gram-positive bacteria. Among the twenty FtsZ inhibitors examined in various assays, **A3** was identified to exhibit excellent antibacterial activity against *S. aureus* (MIC = 0.5-1 μg/mL), *S. epidermidis* (MIC = 0.25 μg/mL) and *E. faecium* (MIC = 1-8 μg/mL). More importantly, **A3** showed low hemolytic toxicity (IC_5 = 64 μg/mL) and was found not readily to induce drug resistance. **A3** at 2-8 μg/mL promoted the polymerization of FtsZ and interrupted the bacterial division. Furthermore, the ligand-FtsZ interaction study conducted with circular dichroism and molecular docking revealed that **A3** induced secondary structure changes of FtsZ protein upon binding to the interdomain cleft of the protein. **A3** is thus a potent inhibitor of FtsZ and shows potential to be used as a new antibacterial agent against drug-resistant bacteria.

Keywords: 1-Methylquinolinium derivatives, FtsZ inhibitor, Antibacterial activity, Mechanism of action, Drug resistance.

1. Introduction

The discovery of penicillin, the first antibiotic found in 1928, has saved innumerable lives. Beta-lactam antibiotics are regarded as one of the most important scientific discoveries in the 20th century [1, 2]. Nonetheless, the abuse and misuse of antibiotics accelerated the emergence cycle of drug resistance. For example, penicillin-resistant *S. aureus* (PRSA) was reported soon after penicillin applied to clinical medicine [3]. Currently, many drug-resistant bacteria including methicillin-resistant *S. aureus* (MRSA), vancomycin-resistant *E. faecium* (VRE) and the multidrug-resistant bacterial strains are commonly found in clinical settings [4-7] and these bacteria make the clinical antibiotics incapable of treating bacterial infections. The threat of drug-resistant bacteria or superbugs renders an urgent need to develop new types of antibacterial agents to solve the antibiotic resistance crisis.

To search for new compounds selectively binding to essential proteins of bacterial cell cycle rather than penicillin-binding proteins is a promising strategy to develop a new class of antibacterial agents. With respect to the mechanism of bacterial cell division, it involves complicated dynamic and biological processes and requires many functional division proteins, which could be the potential antibacterial drug targets [8, 9]. Filamentous temperature sensitive mutant Z (FtsZ) is one of the essential proteins required for bacterial cell division and is highly conserved in bacteria [10]. Therefore, it is an ideal drug target for new antibiotic development. Since FtsZ is the first protein that reaches the division site, the interruption of the function of FtsZ may cause bacterial death [11-13]. Recent studies have also demonstrated that some small organic molecules such as sanguinarine, berberine, PC190723 and Zantrin Z3 (**Fig. 1**) are the potent inhibitors of FtsZ [14-20]. However, only very few FtsZ inhibitors including TXA707 and TXA709 have been reported for clinical trial [19, 21-23], which indicates that the development of effective inhibitors targeting FtsZ for clinical use remains a challenge.

Among the active FtsZ inhibitors reported recently, sanguinarine [14], berberine [15, 16], PC190723 [18] and Zantrin Z3 [20] are the hetero-bicyclic or hetero-polycyclic organic compounds that exhibit potent antibacterial activities. Our recent results further indicate that the 1-methylquinolinium is an active hetero-bicyclic scaffold for FtsZ inhibitor development [24, 25]. In addition, we have previously found that the hetero-bicyclic indolyl-quinolinium derivatives **c9** and

BIMQ [26, 27] (**Fig. 2**) are the effective pharmacophore for FtsZ inhibitor development. A recent study with the use of semi-synthetic kaempferol derivatives reported that the introduction of amine substituents with low *pKa* values into flavone scaffold was unfavourable to antibacterial activity [28]. Based on this, we tried to introduce *N,N*-dimethylaniline (with basic nitrogen) into the 1-methylquinolinium ring to replace the indole substituent (with acidic nitrogen) and that may be able to enhance the antibacterial activity. In addition, the effect of substituent groups at the 2- and 4-position of the 1-methylquinolinium ring for structure-activity relationship (SAR) study has not been systemically investigated. In the present study, we therefore focused on the structural design and advancement at the 2- and 4-position of the 1-methylquinolinium and to understand the SAR of antibacterial activity targeting FtsZ protein. In the molecular design, two series of structurally similar compounds, **A** series and **B** series (**Fig. 2**), with different substituent groups at the 2- and 4-position of the 1-methylquinolinium ring, were synthesized for comparison.

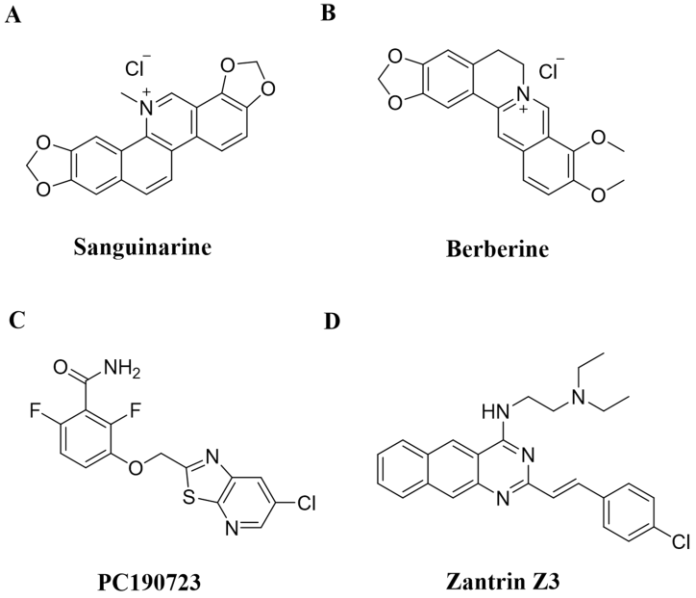

Fig. 1. Molecular structures of some recent reported FtsZ inhibitors: (A) sanguinarine, (B) berberine, (C) PC190723, (D) Zantrin Z3.

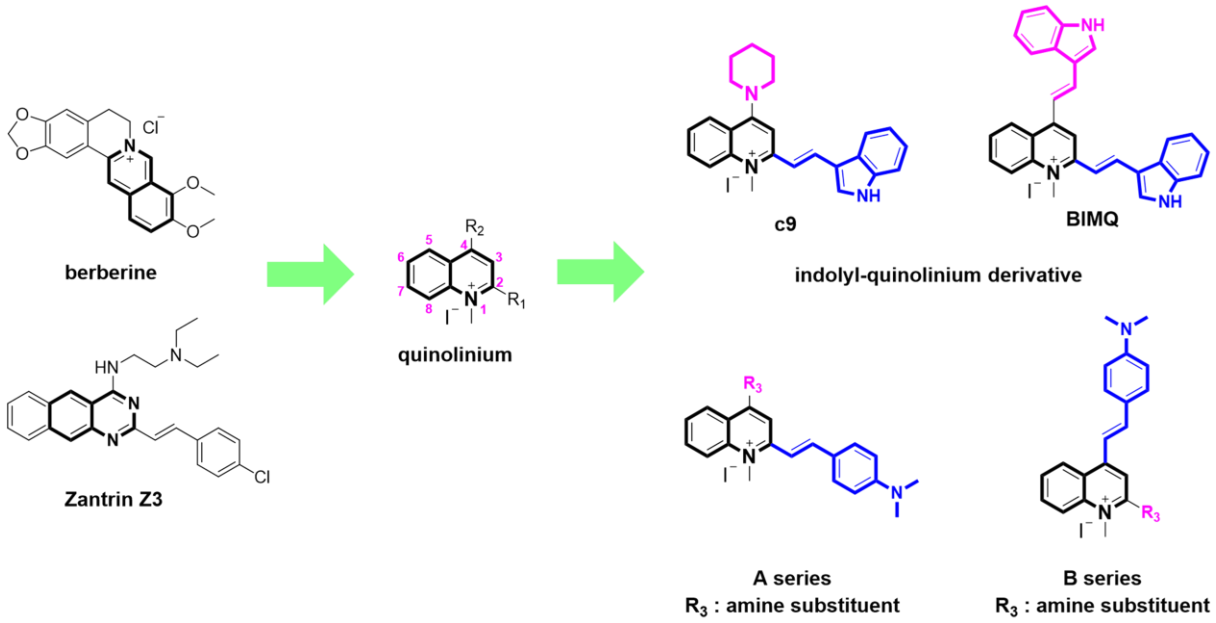

Fig. 2. The structural design of the quinolinium-based derivatives targeting FtsZ. The core heterobicyclic skeleton of 1-methylquinolinium (black), the varied substituent groups (pink), and the substituent of 4-(dimethylamino)styryl (blue).

2. Results and Discussion

2.1 Synthesis of 1-methylquinolinium-based derivatives A1-A10, B1-B10

The compounds **A1-A10**, **B1-B10** (**Scheme 1**) were synthesized and purified according to the reported procedures [26, 29]. Intermediates **2a** and **5a** were obtained by the reaction of 4-chloro-2-methylquinoline or 2-chloro-4-methylquinoline with iodomethane. The reaction of **2a** or **5a** with a selected amine gave **3a-3i** and **6a-6i**, respectively. These compounds were further reacted with 4-dimethylaminobenzaldehyde to obtain the inhibitors **A1-A9**, **B1-B9**. For intermediates **2b** and **5b**, the compounds were obtained by the reaction of 2-methylquinoline or 4-methylquinoline with iodomethane. After obtaining the intermediates, **2b** and **5b** were further reacted with 4-dimethylaminobenzaldehyde to obtain **A10** and **B10**. All compounds were characterized by ^{1}H NMR, ^{13}C NMR, HRMS and HPLC (**Fig. S10-S29**). The *E*-isomers were the major products of the synthesis and were purified with column chromatography. HPLC analysis showed that the purity of the isolated compounds were higher than 95%. The compounds were designed to bear a positively charged quinolinium fragment for electrostatic interactions, a non-polar group of styryl fragment for non-polar interactions and a flexible or rigid amine group for hydrogen bond

interactions to enhance the affinity with the drug target.

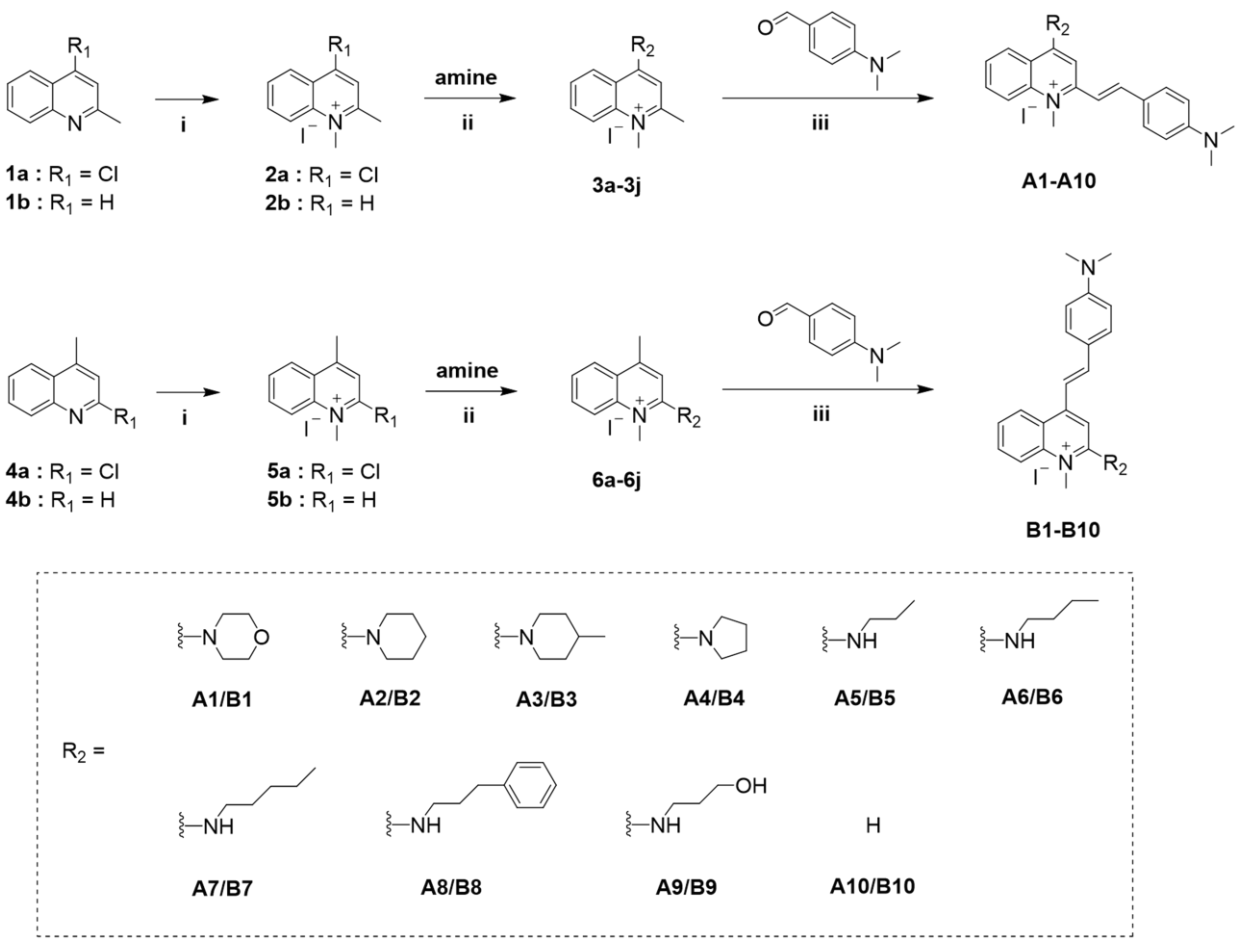

Scheme 1. Synthetic routes to the compounds of **A** series and **B** series. Reagents and conditions: (i) iodomethane, sulfolane, 60 ℃, overnight; (ii) the reaction with a selected amine, acetonitrile, 60 ℃, overnight; (iii) aldehyde in n-butanol, 4-methylpiperidine, 100 ℃, 8 h.

2.2 *In vitro* antibacterial activity of the derivatives

The antibacterial activity of 1-methylquinolinium-based derivatives (**A1-A10**, **B1-B10)** was evaluated using the broth microdilution method. The structural difference between two series (**A** series and **B** series) of compounds is the amine group substituted at the C-2 and C-4 position of the 1-methylquinolinium scaffold. The MIC results summarized in **Table 1-3** revealed that the compounds against Gram-positive bacteria generally showed much better antibacterial activity than that of Gram-negative bacteria. Interestingly, in terms of MIC values, **A10** and **B10** only bearing an *N,N*-dimethylaniline substituent at either C-2 or C-4 position exhibited similar antibacterial activity, which may indicate that the substitution position of *N,N*-dimethylaniline did not cause

significant influence in the antibacterial activity. Furthermore, by comparing the MIC values of the compounds with the same amine-substituent at C-2 or C-4 position, it was found that the antibacterial activity of **A** series was approximately 2-16 times better than **B** series. The results suggest that the substituent groups at C-4 position (**A** series) were more potent than that at C-2 position (**B** series). We thus speculated that the substituents at the C-4 position of the inhibitor could be a critical site to influence the structure and function of FtsZ protein. By comparing the substituent groups, it was found that morpholine (**A1**/**B1**) and 3-aminopropanol (**A9**/**B9**) groups containing oxygen atom (MIC = 16-64 μg/mL) showed much weaker antibacterial activity than piperidine (**A2**/**B2**) and *N*-propylamine (**A5**/**B5**) groups bearing no oxygen atom (MIC = 1-8 μg/mL).

In the MIC screening assays, four compounds **A3**, **B3**, **A2** and **A7** were found showing high antibacterial activity among the twenty derivatives. In particular, **A3** is the best one and inhibits effectively the growth of *S. aureus* (MIC = 0.5-1 μg/mL). In addition, **A3** against MRSA was found comparable to vancomycin but it was weaker than rifampin. The compound also showed better antibacterial activity against *S. epidermidis* and *E. faecium* including the drug-resistant bacterial strains. Comparing with Gram-positive bacteria, **A3** generally display less antibacterial potency against most Gram-negative bacteria tested such as *E. coli* ATCC 8739 (MIC = 64 μg/mL) and *P. Aeruginosa* ATCC 27853 (MIC > 64 μg/mL). We speculated that the low bacterial membrane permeability of the compound may be a key factor that probably weakens the antibacterial activity against Gram-negative bacteria [30]. We thus used polymyxin B nonapeptide (PMBN) to enhance the outer membrane permeability of Gram-negative bacteria [31-33]. From the results shown in **Table S1**, we found that PMBN at 256 μg/mL did not inhibit the strains of *E. coli* ATCC 25922, *E. coli* ATCC 8739, *A. baumannii* ATCC 19606 and *P. aeruginosa* ATCC 27853; however, by combining the inhibitors (**A3**, **B3**, **A2** and **A7**) with PMBN (20 μg/mL), the MIC against the Gram-negative bacteria was significantly reduced to 1-8 μg/mL. The results indicate that the permeability of the bacterial outer membrane may be a critical factor reducing the antibacterial activity of the compounds against Gram-negative bacteria.

153 **Table 1.** The minimum inhibitory concentration (MIC) of compounds against *Staphylococcus*
154 *aureus* (μg/mL).

	S. aureus **ATCC 29213**	***S. aureus*** **ATCC 43300[a]**	***S. aureus*** **ATCC 33592[a]**	***S. aureus*** **ATCC BAA-1720[a]**	***S. aureus*** **Mu50[b]**
A1	32	64	64	64	32
A2	1	1	1	2	2
A3	1	1	0.5	1	1
A4	1	2	1	8	1
A5	8	8	4	4	8
A6	4	4	2	2	4
A7	2	2	2	1	4
A8	2	2	2	2	4
A9	32	64	32	64	16
A10	16	nd	nd	nd	nd
B1	32	>64	64	>64	32
B2	2	4	8	4	4
B3	2	4	4	4	4
B4	4	16	16	16	8
B5	>64	32	>64	16	32
B6	32	16	32	16	16
B7	8	8	8	8	8
B8	4	4	4	4	4
B9	>64	>64	64	64	64
B10	16	nd	nd	nd	nd
Cip[c]	0.25	2	0.125	>64	1
Amp[c]	>64	>64	64	>64	0.125
Van[c]	1	1	2	0.5	32
Rif[c]	0.5	<0.125	>64	<0.125	0.125

155 [a] Methicillin-resistant strain. [b] Vancomycin-intermediate strain. [c] Cip: ciprofloxacin, Amp:
156 ampicillin, Van: vancomycin, Rif: rifampin.
157

158 **Table 2.** The minimum inhibitory concentration (MIC) of compounds against Gram-positive
159 bacteria strains (μg/mL).

	S. epidermidis ATCC 12228	*B. subtilis* CMCC (B) 63501	*E. faecium* ATCC 49624	*E. faecalis* ATCC 29212	*E. faecium* ATCC 700221[a]	*E. faecium* VRE Strain[a, b]
A1	16	32	8	>64	16	32
A2	1	2	8	4	1	4
A3	0.25	4	8	2	1	4
A4	1	4	4	2	2	4
A5	2	16	16	4	4	8
A6	2	8	16	2	4	8
A7	1	4	8	4	4	4
A8	2	4	4	8	4	4
A9	8	>64	8	16	16	>64
A10	16	64	8	>64	nd	nd
B1	16	16	8	>64	32	>64
B2	1	4	8	16	2	8
B3	1	8	16	16	2	16
B4	2	16	16	64	8	16
B5	32	16	32	64	16	16
B6	16	8	16	32	8	8
B7	8	8	8	16	8	8
B8	4	2	4	4	4	4
B9	64	32	>64	>64	64	64
B10	16	64	16	>64	nd	nd
Cip[c]	1	0.25	32	4	>64	nd
Amp[c]	>64	4	2	1	0.25	>64
Van[c]	>64	0.25	1	2	1024	>64
Rif[c]	1	0.125	<0.125	0.125	<0.125	8

160 [a] Vancomycin-resistant strain. [b] Clinically isolated strain. [c] Cip: ciprofloxacin, Amp: ampicillin,
161 Van: vancomycin, Rif: rifampin.
162

Table 3. The minimum inhibitory concentration (MIC) of compounds against Gram-negative bacteria strains (μg/mL).

	E. coli ATCC 25922	*E. coli* ATCC 8739	*E. coli* ATCC BAA 2469[a]	*A. baumannii* ATCC 19606[b]	*P. aeruginosa* ATCC 27853[c]	*K. pneumoniae* ATCC BAA 2470[a]
A1	>64	>64	>64	>64	>64	>64
A2	16	64	64	64	>64	>64
A3	8	64	64	>64	>64	>64
A4	4	16	64	32	>64	>64
A5	32	>64	>64	>64	>64	>64
A6	32	>64	>64	>64	>64	>64
A7	64	>64	>64	>64	>64	>64
A8	>64	>64	>64	>64	>64	>64
A9	>64	>64	>64	>64	>64	>64
B1	>64	>64	>64	>64	>64	>64
B2	16	32	64	>64	>64	>64
B3	32	64	64	>64	>64	>64
B4	16	32	64	>64	>64	>64
B5	>64	>64	>64	>64	>64	>64
B6	>64	>64	>64	>64	>64	>64
B7	>64	>64	>64	>64	>64	>64
B8	>64	>64	>64	>64	>64	>64
B9	>64	>64	>64	>64	>64	>64
Cip[d]	0.125	<0.125	>64	64	1	>64
Amp[d]	2	16	>64	>64	>64	>64
Van[d]	>64	>64	>64	>64	>64	>64
Rif[d]	2	8	>64	>64	>64	>64

[a] NDM-1 expressing strain. [b] Multi-drug resistant strain. [c] Penicillin-susceptible strain. [d] Cip: ciprofloxacin, Amp: ampicillin, Van: vancomycin, Rif: rifampin.

2.3 The study of bactericidal and bacteriostatic effects

The MBC values of the screened potent compounds (**A3**, **B3**, **A2** and **A7**) against *S. aureus*, *B. subtilis* and *E. faecium* were investigated. The strains including *S. aureus* ATCC 29213, *S. aureus* ATCC 43300, *B. subtilis* CMCC (B) 63501 and *E. faecium* ATCC 700221 were tested. According to the CLSI standard [34], the bactericidal effect was observed when the ratio of MBC/MIC was ≤ 2, while the bacteriostatic effect was observed when the ratio of MBC/MIC was ≥ 4. The MBC results (**Table 4**) revealed that these compounds were bacteriostatic agents for *S. aureus* and *E. faecium*, which were similar to the previously reported thiazole-quinolinium derivatives and the antibiotic Teicoplanin [35, 36]. On the other hand, the compounds, similar to a clinical antibiotic nalidixic acid [37], were bactericidal agents against *B. subtilis*.

Table 4. MBCs and MBC/MIC ratios of selected compounds against four bacterial strains.

	MBC (μg/mL)	MIC (μg/mL)	MBC/MIC
***S. aureus* ATCC 29213**			
A3	8	1	>4
B3	16	2	>4
A2	8	1	>4
A7	8	2	4
***S. aureus* ATCC 43300**			
A3	8	1	>4
B3	32	4	>4
A2	4	1	4
A7	8	2	4
***B. subtilis* CMCC (B) 63501**			
A3	4	4	1
B3	16	8	2
A2	4	2	2
A7	4	4	1
***E. Faecium* ATCC 700221**			
A3	4	1	4
B3	8	2	4
A2	4	1	4
A7	8	4	2

2.4 Time-killing kinetics of the inhibitor against a clinical isolate *S. aureus* ATCC 29213

The potent compound **A3** was further investigated to understand its time-killing kinetics against *S. aureus* ATCC 29213. The time-killing curve (**Fig. 3**) revealed that *S. aureus* was increased rapidly and reached 10^{11} CFU/mL without applying **A3**. However, with the addition of **A3** at 1×, 2×, and 4× MIC concentrations, respectively, the viable counts of bacteria decreased to 10^3–10^4 CFU/mL after 8 h and then remained steady. It was found that the higher the concentration of **A3** used, the faster the rate of colonies decreased in the assay. Moreover, when the concentration of **A3** used was at 8× MIC, the bacterial counts were significantly reduced to below 10^3 CFU/mL after 8 h. Finally, the viable bacteria were no longer detectable after 24 h incubation. The results suggested that **A3** at 1×, 2×, 4× MIC concentrations inhibited the growth of *S. aureus* in a bacteriostatic mode and, at 8× MIC concentration, it killed *S. aureus*. The finding was in accord with the MBC results [27, 38].

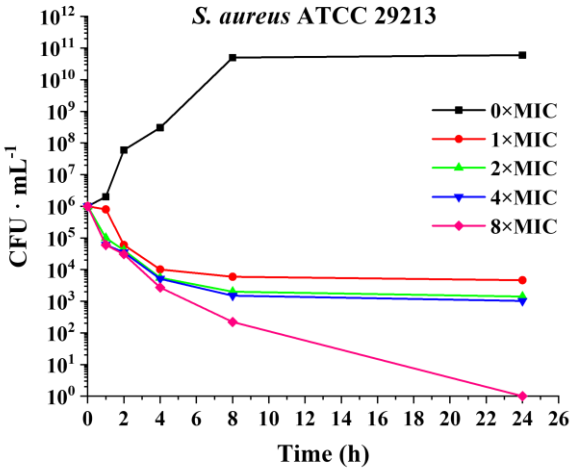

Fig. 3. Time-killing curves of **A3** against *S. aureus* ATCC 29213. The assays were conducted at different compound concentrations: 0× MIC (1% DMSO) (black), 1× MIC (red), 2× MIC (green), 4× MIC (blue), and 8× MIC (pink).

2.5 Synergistic effects with methicillin against MRSA

The checkboard assay was used to investigate the synergistic effect of compounds **A3**, **B3**, **A2** and **A7** with methicillin against MRSA strains. Fractional inhibitory concentration (FIC) index ≤ 0.5 was considered as synergism; 0.5-2 was considered as for additive effect, and > 2 was considered as antagonism [23, 39]. From the results of **Table 5** and **Fig. S1**, it was found that the

MIC values of methicillin against MRSA were reduced to 64 μg/mL when combined with **A3** (2 μg/mL) and **B3** (4 μg/mL), with an FIC index of 0.3125, indicating a synergistic effect. Compounds **A2** and **A7** also exerted similar effects. Therefore, these compounds could restore the antibacterial activity of methicillin against MRSA in a synergistic manner.

Table 5. Synergistic effects of **A3**, **B3**, **A2** and **A7** with methicillin against *S. aureus* ATCC BAA-41.

	FIC index	MIC (μg/mL)	
		alone	in combination
A3	0.3125	8	2
methicillin		1024	64
B3	0.3125	16	4
methicillin		1024	64
A2	0.25	16	2
methicillin		1024	128
A7	0.375	4	0.5
methicillin		1024	256

2.6 Effects of the derivatives on bacterial cell division

FtsZ is highly conserved among bacteria and is an essential protein for bacterial cell division. The interruption of FtsZ function may inhibit the bacterial cell division process. The morphology change of bacterial cells including cell length and/or size is one of the important phenotypes indicating the interruption of FtsZ function. In the present study, *B. subtilis* CMCC (B) 63501 was used to investigate the effect of the compounds on bacterial morphology changes. As shown in **Fig. 4A-B**, the cell length of the bacteria was about 3-5 μm in the control group; however, for the treatment group applying **A3** at 0.5× MIC for 4 h, a significant elongation of the bacterial cell (*B. subtilis*), approximately 70 μm, was observed. Similarly, compounds **A2**, **A7** and **B3** were able to cause the elongation of bacterial cells with a length about 30-50 μm (**Fig. S2**). Furthermore, *S. aureus* was used to conduct the same evaluation (**Fig. 4C-D**). The size of bacterial cells observed in the control group was about 1 μm, while after treating with **A3**, **B3**, **A2** and **A7** at 0.5× MIC, an enlargement of cell size was observed clearly. These results indicate that the compounds may target

FtsZ and exert significant effects on the inhibition of bacterial cell division.

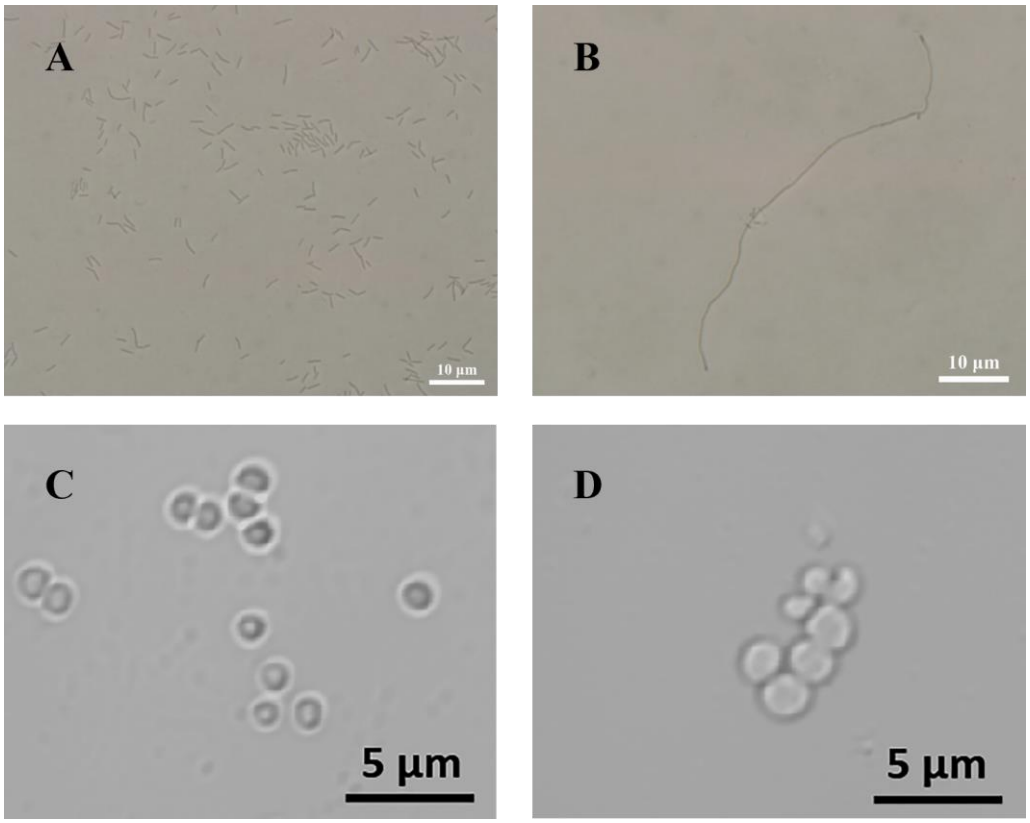

Fig. 4. The effect on the morphology of *B. subtilis* CMCC (B) 63501 and *S. aureus* ATCC 29213 in the absence (A, C) and the presence of **A3** (B, D). Scale bar for *B. subtilis* is 10 μm and for *S. aureus* is 5 μm.

2.7 Effects of the derivatives on the FtsZ function

Some FtsZ inhibitors such as PC190723, Zantrins, berberine and its derivatives [14, 16, 18] were reported to hinder the bacterial division through the interruption of the function of FtsZ protein. Our compounds may also target FtsZ and interrupt its function. *S. aureus* FtsZ was used to study the *in vitro* effect of the compounds on the polymerization of FtsZ. In the assays, both **A3** and **B3** were able to promote FtsZ polymerization with respect to the remarkably increased A_{340} values compared with the control using DMSO (**Fig. 5**). Notably, **A3** showed much stronger enhancement effect than **B3**. The result may suggest that the compound (**A3**) with a cyclic amine group substituted at C-4 position of the 1-methylquinolinium ring could render better promotion effects on FtsZ polymerization. We further monitored the A_{340} changes of compounds **A3**, **B3**, **A2** and **A7** at a gradient concentration from 2 μg/mL to 8 μg/mL (**Fig. S3**). It was found that the

compounds gave different degrees of enhancement in FtsZ polymerization. In general, the enhancement was found in a concentration-dependent manner. The promotion effect was also found in accord with the reported compounds such as OBTA, PC190723 and TXA707 [18, 19, 40].

Since the FtsZ polymerization dynamic could also be regulated by GTPase activity, we further analyzed the effect of the compounds (**A3**, **B3**, **A2**, and **A7**) on GTPase activity using the GTPase kit. We found that all the compounds tested had no significant effect on the GTPase activity of *S. aureus* FtsZ (**Fig. 6**). The results were found similar to the reported inhibitors [41, 42] including the thiazole-quinolinium derivatives [35]. It could be due to the compounds bound to the interdomain cleft of FtsZ that may only enhance the polymerization of FtsZ protein but has no effect on interfering GTPase activity.

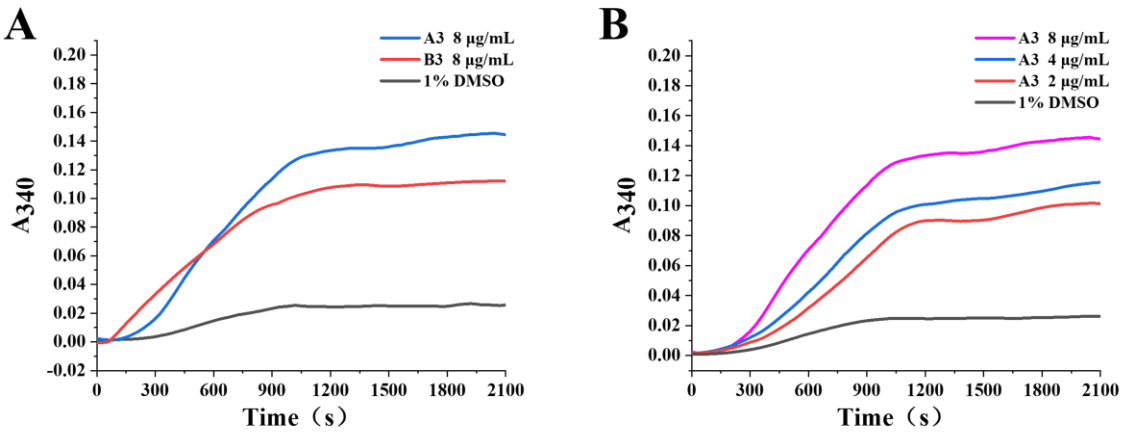

Fig. 5. (A) The effect of compounds **A3** and **B3** at 8 μg/mL on the polymerization of FtsZ. (B) The effect of compound **A3** at the concentration from 2 to 8 μg/mL on the polymerization of FtsZ.

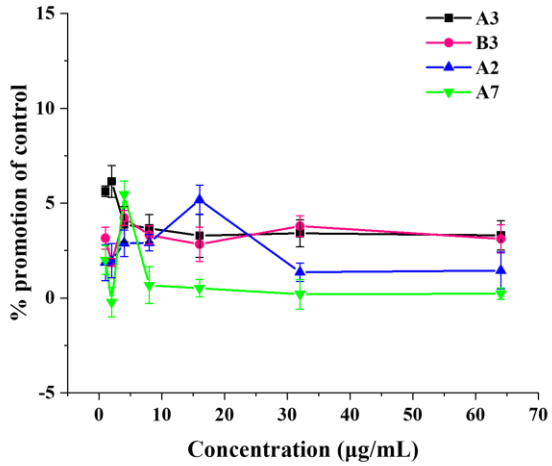

Fig. 6. The effect of **A3**, **B3**, **A2** and **A7** on the GTPase activity of FtsZ.

2.8 Interaction study of the derivatives with FtsZ protein

The secondary structure of *S. aureus* FtsZ upon interacting with the inhibitor was tested by circular dichroism (CD) spectra. The spectroscopic data were processed by the software Chirascan Pro-Data Viewer and CDNN. The results (**Fig. 7A**) revealed that FtsZ with DMSO (control) contained 30.5% α-helix, 17.4% β-turn, 34.5% random coil and 17.6% other structures. After the treatment with **A3** at 8 μg/mL, α-helix was increased to 41%, β-turn was decreased to 15.5%, random coil was decreased to 28.4%, and the other structures were decreased to 15.1% (**Table S2**). Similarly, the CD spectra of FtsZ were changed after **B3**, **A2** or **A7** treatment (**Fig. 7B**), suggesting that the content of secondary structures were changed (**Table S2**). The above results indicate that the compounds may interact with FtsZ protein and consequently cause the change of the secondary structure of the protein that results in breaking the balance of FtsZ polymerization [43]. The protein function was therefore interrupted.

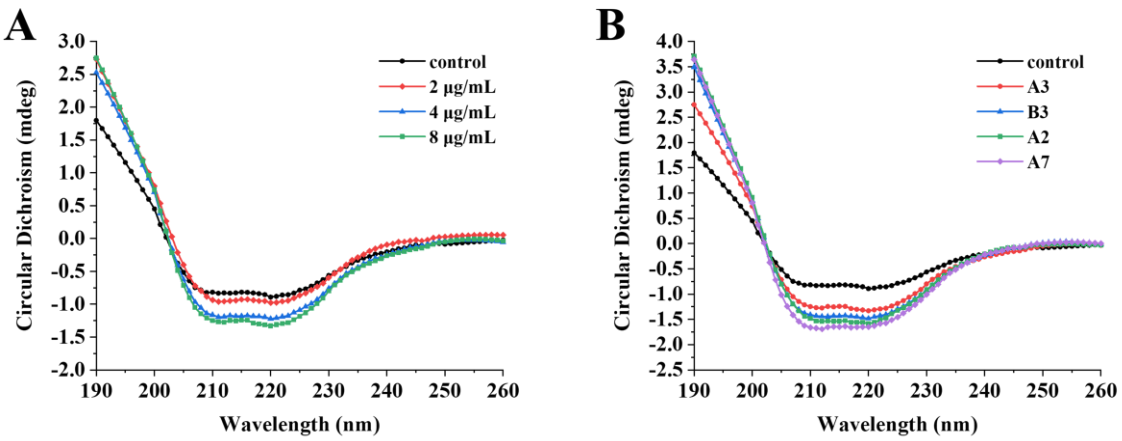

Fig. 7. The CD spectra of FtsZ (A) in the absence and presence of **A3** at a concentration from 2 to 8 μg/mL, (B) in the presence of 8 μg/mL **A3**, **B3**, **A2** and **A7**.

In addition, fluorescence titration method was also conducted to investigate the protein-ligand interaction. The detection of the changes in the intrinsic fluorescence of the compounds in the presence of *S. aureus* FtsZ protein may indicate the protein-ligand interaction occurred [44, 45]. As shown in **Fig. S5**, the fluorescence intensity was increased markedly as FtsZ was gradually added and the signal increased was in a concentration-dependent manner. The observation suggests that the compound may interact with FtsZ in solution. The equilibrium binding constants (K_{eq}) of **A3**, **B3**, **A2** and **A7** with FtsZ were estimated to be 2×10^5 M^{-1} - 4×10^5 M^{-1} (**Table 6**). In addition,

isothermal titration calorimetry (ITC) titrations were performed to analyze the thermodynamic interaction of ligand-FtsZ. The results demonstrated that these compounds interacted with FtsZ spontaneously (**Table 6** and **Fig. S6**) with the dissociation constant (K_D) at micro-molar level [15].

Table 6. The binding constants (K_{eq}) and dissociation constants (K_D) of FtsZ with the selected compounds.

	A3	**B3**	**A2**	**A7**
Binding constant K_{eq} **(×10^5 M^{-1})**	4.41	2.08	2.02	2.01
Dissociation constant K_D **(μM)**	3.84	3.86	2.49	2.38

2.9 Prediction of the binding mode of the 1-methylquinolinium-based derivatives with FtsZ

Based on the results obtained from biological assays, **A3** could be a potential inhibitor of FtsZ. The possible binding modes and binding sites of the compound with FtsZ were further studied with molecular docking. By comparing the biological activity of **A3** with PC190723, both compounds could increase FtsZ polymerization. From **Fig. 8A**, **A3** was predicted to bind to the hydrophobic interdomain cleft formed by H7-helix, T7-loop, and C-terminal β-sheet, which was consistent with the reported binding pocket of PC190723 that was confirmed by the crystal structure of *S. aureus* FtsZ in complex with PC190723 [46]. This could provide an explanation that **A3** does not affect the GTPase activity. The 2D diagram (**Fig. 8B**) showed a number of hydrophobic interactions between **A3** and the residues (Leu200, Met226, Ile228, and Val297) of FtsZ. Moreover, amide-π stacking, sometimes important for ligand binding [47], could be found between the 1-methylquinolinium moiety and the residues including Gln192, Gly227 and Thr309. In addition, a carbon hydrogen bond interaction was predicted between the amine carbon chain and Gln192. A carbon hydrogen bond was also predicted with the residues of Val203, Val207 and Asn208. Furthermore, a large number of amino acid residues, such as Asp199, Gly205, Asn263 and Ile311, were predicted interacting with **A3** through van der Waals forces.

From the docking results, **A3** may insert into the cleft with a slab configuration similar to that

of PC190723 [48]. The interaction between FtsZ and **A3** may also involve a number of amino acid residues that are the same as those found in the FtsZ-PC190723 interaction. The *N,N*-dimethylaniline substituent of **A3** is predicted directly to interact with the T7-loop (Leu200, Val203, and Asn208), which is similar to the interaction observed in PC190723 with difluorobenzamide substituent. In addition, both the 1-methyl quinolinium ring and the 4-methylpiperidine substituent show hydrophobic interactions with H7-helix (Gln192) and β-sheet (Met226 and Ile228), which are similar to the interaction observed in the thiazopyridine ring of PC190723. However, there is an obvious difference found between **A3** and PC190723 interacting with FtsZ. Gly193, one of the two amino acids that accounted for 90% of all PC190723-resistant MRSA mutations, has a hydrophobic interaction with PC190723; interestingly, it interacts with **A3** through van der Waals force [18, 48]. Furthermore, the predicted binding mode between **B3** and FtsZ (**Fig. S7**) was similar to that of **A3**. Nonetheless, we observed four amide-π stacked interactions of Gln192, Gly227 and Val203 with **A3** but not with **B3**. There is only one amide-π stacking between **B3** and Asp199.

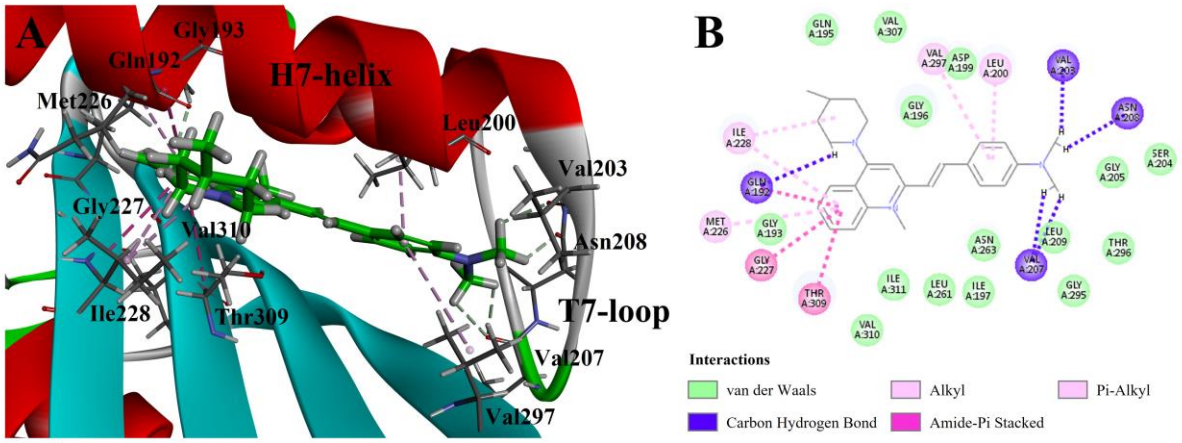

Fig. 8. Predicted binding modes of **A3** with *S. aureus* FtsZ. (A) **A3** bound to the C-terminal interdomain cleft of FtsZ. (B) Predicted interactions between **A3** and the amino acids of FtsZ.

2.10 Toxicity of the derivatives

The hemolytic toxicity of the quinolinium-based derivatives was determined against erythrocytes from Kunming mice. Triton X-100 (0.008%-1%) was used as the reference. The hemolytic toxicity of other quinolinium-based derivatives was summarized in **Fig. S8** and **Table S3** for comparison. Among the compounds tested, both **A3** (IC_5 = 64 μg/mL) and **B3** (IC_5 = 32 μg/mL) have low hemolytic toxicity (**Fig. 9A**) and have better IC_5/MIC selectivity against mice

erythrocytes and *S. aureus* 29213 (**Table S3**).

The cytotoxicity of the compounds with better antibacterial activity was determined against the mouse fibroblasts (L929) cells and human renal tubular (HK-2) cells. The IC_{50} results showed that the cytotoxicity of **A3** was slightly lower than **B3** (**Fig. 9B**). Furthermore, the selective index (SI = IC_{50}/MIC) indicated that **A3** has better selectivity than **B3**, which is similar to the results showed in the hemolytic toxicity. Interestingly, **A3** bearing a 4-methylpiperidyl group substituted at the C4-position of the 1-methylquinolinium ring is less toxic than that of **B3** (bearing a 4-methylpiperidyl group substituted at C2-position). In addition, **A3** exhibits better antibacterial activity.

A

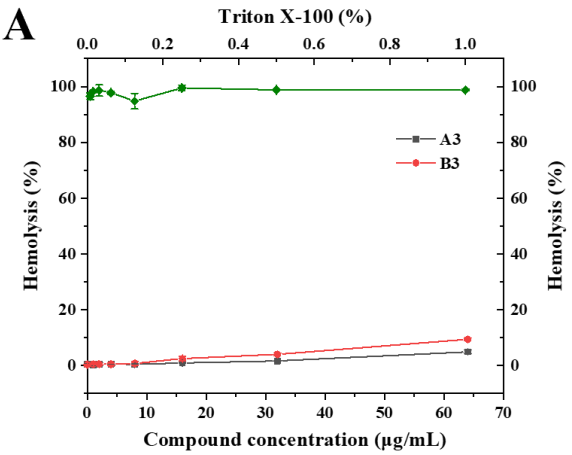

B

	MIC[a] (μg/mL)		IC_{50} (μg/mL)	
	A3	**B3**	**A3**	**B3**
L929	1	2	12.77	11.30
HK-2	1	2	9.42	8.89

[a] MIC value against *S. aureus* ATCC 29213.

Fig. 9. (A) Hemolytic toxicity of compounds **A3** and **B3**. The erythrocytes were treated with compounds (1-64 μg/mL) or Triton X-100 (0.008%-1%). (B) Cytotoxicity of compounds **A3** and **B3** on L929 and HK-2.

2.11 Drug resistance of the 1-methylquinolinium-based derivatives

To evaluate the drug-resistance of **A3** and **B3** against *S. aureus* ATCC 29213 and *B. subtilis* CMCC (B) 63501, three antibiotics (vancomycin, ciprofloxacin, and rifampin) were used as the control. After 35-passage incubation at sub-inhibitory concentration (0.5×MIC), the results (**Fig. 10**) indicated that the MIC of **A3** and **B3** against *S. aureus* ATCC 29213 was increased only 8-fold, which is much less than the controls (128-fold for vancomycin, 512-fold for ciprofloxacin and 4096-fold for rifampin). Similar results were also obtained in *B. subtilis* CMCC (B) 63501 (**Fig. S9**). With respect to the results, both **A3** and **B3** could effectively delay the induction of drug

resistance.

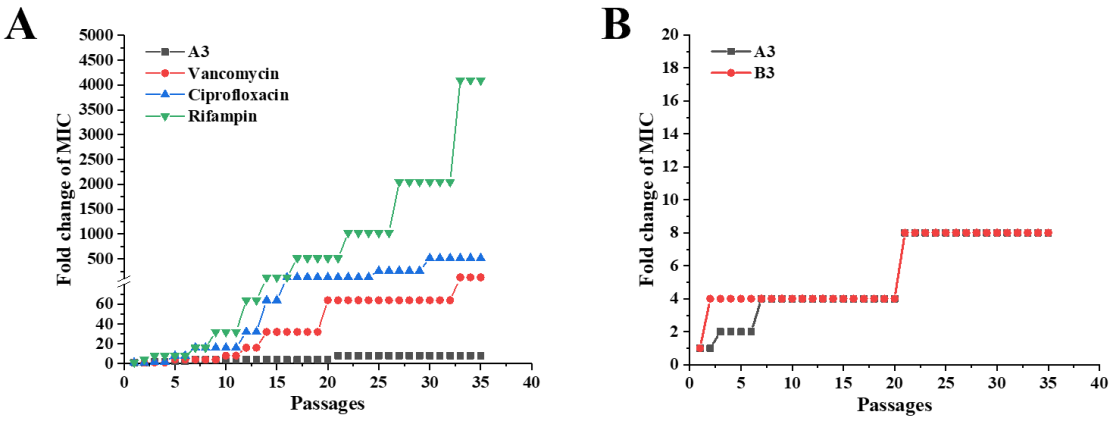

Fig. 10. Bacterial resistance evaluation of (A) **A3**, vancomycin, ciprofloxacin, and rifampin, (B) compounds **A3** and **B3** against *S. aureus* ATCC 29213.

3. Conclusion

In conclusion, two series of quinolinium-based derivatives were systematically designed and synthesized for the study of the effect of substituent groups at the C4-position (**A** series) and C2-position (**B** series) of the 1-methylquinolinium scaffold on the antibacterial activity targeting FtsZ. Compared to **B** series, the results generally suggested that **A** series exhibited better antibacterial activity against most of the bacteria including the antibiotic-resistant bacteria and showed lower cytotoxic. Among the compounds, **A3** showed stronger antibacterial activity than **B3** against Gram-positive bacteria (0.5-8 μg/mL) including the common clinically resistant strains such as MRSA (0.5-1 μg/mL), VISA (1 μg/mL) and VRE (1-4 μg/mL). In addition, **A3** exhibited weak activity against Gram-negative bacteria but it could be improved significantly by combining with PMBN. The mechanism study suggested that **A3** significantly caused cell elongation of *B. subtilis* by enhancing FtsZ polymerization, while the compound did not affect the GTPase activity. The results of circular dichroism spectroscopy, fluorescence titration, isothermal titration calorimetry, and molecular docking study indicate that **A3** may be a potent FtsZ inhibitor with high affinity and less cytotoxic and shows low tendency to induce drug resistance. Taken together, the quinolinium-based derivatives bearing an amine substituent at the C-4 position of the 1-methylquinolinium may be a potential antibacterial drug targeting FtsZ protein to treat drug-resistant bacteria.

4. Materials and methods

4.1 Chemistry

All the chemicals and reagents in the present study were commercially available, using without further purification. All the NMR spectra were obtained by a Bruker AVANCE III 400 MHz Superconducting Fourier Nuclear Magnetic Resonance Spectrometer, with 400 MHz for ^{1}H and 101 MHz for ^{13}C. High-resolution mass spectrometry (HRMS) was obtained by Aglient 7250 TOF. INESA micro-melting point apparatus SGW X-4A was used for the melting point measurements. High performance liquid chromatography (HPLC) analysis was performed by SHIMADZU LC-16 system with Diamonsil C18 column (250 × 4.6 mm, 5 μm) at UV 225 nm detection, for testing the purity and water solubility of the compounds.

4.2 Preparation of intermediates (2a-2b and 5a-5b)

The intermediates **2a** and **5a** were synthesized as described in the previous study [29]. 4-chloro-2-methylquinoline (0.2 g, 1.126 mmol) or 2-chloro-4-methylquinoline (0.2 g, 1.126 mmol) and iodomethane (0.5 g, 3.378 mmol) were dissolved into tetramethylene sulfone (5 mL). After reacting overnight at 60 ℃, the mixture was cooled to room temperature (RT) and precipitated by the addition of ethyl acetate (15 mL). The crude products were washed with ethanol to gain intermediates **2a** and **5a**, yields were 81.8% and 79.6%, respectively.

Intermediates **2b** and **5b** were synthesized by the reaction of 2-methylquinoline or 4-methylquinoline with iodomethane. The synthesis method was similar to that of intermediates **2a** and **5a**, yields were 75.9% and 77.3%, respectively.

4.3 General synthetic procedure of compounds A1-A10, B1-B10

Intermediates **2a** or **5a** (0.2 mmol) and a selected amino (morpholine, piperidine, 4-methylpiperidine, pyrrolidine, *N*-propylamine, *N*-butylamine, *N*-amylamine, 3-phenylpropylamine, 3-aminopropanol) (1 mmol) were mixed in acetonitrile (5 mL). The mixture was stirred and refluxed overnight at 60 ℃, ethyl acetate (15 mL) was then added when TLC showed reaction completed. After shaking and suction filtration, the solid (**3a-3i**, **6a-6i**) was washed by ethyl acetate and dried in vacuum for the next step. The solid (**3a-3i**, **6a-6i**) and 4-dimethylaminobenzaldehyde were dissolved with *n*-butanol. The mixture was stirred and refluxed at 100 ℃ for 8 h. When reaction was completed, the reaction mixture was cooled to room temperature and then ethyl acetate

was added. After standing for 30 min, crude products were collected by suction filtration. The target compounds (**A1**-**A9**, **B1**-**B9**) were obtained by recrystallization in ethanol.

Intermediates **2b** or **5b** and 4-dimethylaminobenzaldehyde were mixed into *n*-butanol and then the reaction was conducted at 100 ℃ for 8 h. After the reaction was completed, the isolation of **A10** and **B10** were carried out with the same procedures described above.

4.3.1 (*E*)-2-(4-(dimethylamino)styryl)-1-methyl-4-morpholinopyridin-1-ium (A1).

Brown solid with yield 86.7%; Melting point: 289.7-293.3 ℃; ^{1}H NMR (400 MHz, DMSO-d_6) δ 8.28 (d, J = 8.4 Hz, 1H), 8.16 (d, J = 6.9 Hz, 1H), 8.01 (t, J = 7.2 Hz, 1H), 7.95 (d, J = 15.6 Hz, 1H), 7.77 (d, J = 9.0 Hz, 2H), 7.72 (t, J = 8.2 Hz, 1H), 7.50 (s, 1H), 7.41 (d, J = 15.6 Hz, 1H), 6.81 (d, J = 9.0 Hz, 2H), 4.23 (s, 3H), 3.90 (s, 4H), 3.72 (s, 4H), 3.05 (s, 6H) ppm. ^{13}C NMR (101 MHz, DMSO-d_6) δ 159.40, 155.44, 152.56, 145.50, 141.22, 133.97, 131.26, 126.81, 126.61, 123.03, 120.29, 119.66, 113.50, 112.25, 105.17, 66.29, 52.46, 38.49 ppm. HRMS *m/z*: calcd for $C_{24}H_{28}N_3O^+$, $[M\text{-}I]^+$ = 374.22269, found 374.22274. HPLC analysis: retention time at 2.780 min (MeOH/H_2O = 50:50 v/v), purity 95.3%.

4.3.2 (*E*)-2-(4-(dimethylamino)styryl)-1-methyl-4-(piperidin-1-yl)quinolin-1-ium (A2).

Brown solid with yield 87.9%; Melting point: 232.2-235.7 ℃; ^{1}H NMR (400 MHz, DMSO-d_6) δ 8.24 (d, J = 9.0 Hz, 1H), 8.07 (d, J = 9.8 Hz, 1H), 8.02 – 7.95 (m, 1H), 7.88 (d, J = 15.6 Hz, 1H), 7.75 (d, J = 8.9 Hz, 2H), 7.73 – 7.67 (m, 1H), 7.43 (s, 1H), 7.38 (d, J = 15.6 Hz, 1H), 6.79 (d, J = 9.0 Hz, 2H), 4.19 (s, 3H), 3.68 (d, J = 10.3 Hz, 4H), 3.04 (s, 6H), 1.84 (s, 4H), 1.77 (s, 2H) ppm. ^{13}C NMR (101 MHz, DMSO-d_6) δ 159.76, 155.00, 152.41, 144.76, 141.27, 133.84, 131.08, 126.82, 126.30, 123.09, 120.32, 119.51, 113.72, 112.21, 104.64, 53.23, 38.32, 25.88, 24.05 ppm. HRMS *m/z*: calcd for $C_{25}H_{30}N_3^+$, $[M\text{-}I]^+$ = 372.24342, found 372.24400. HPLC analysis: retention time at 2.928 min (MeOH/H_2O = 50:50 v/v), purity 95.1%.

4.3.3 (*E*)-2-(4-(dimethylamino)styryl)-1-methyl-4-(4-methylpiperidin-1-yl)quinolin-1-ium (A3).

Brown solid with yield 90.8%; Melting point: 242.9-246.4 ℃; ^{1}H NMR (400 MHz, DMSO-d_6) δ 8.23 (d, J = 8.9 Hz, 1H), 8.07 (d, J = 8.4 Hz, 1H), 8.01 – 7.95 (m, 1H), 7.88 (d, J = 15.6 Hz, 1H), 7.75 (d, J = 8.9 Hz, 2H), 7.70 (t, J = 7.7 Hz, 1H), 7.43 (s, 1H), 7.38 (d, J = 15.6 Hz, 1H), 6.79 (d, J = 9.0 Hz, 2H), 4.19 (s, 3H), 4.07 (d, J = 13.0 Hz, 2H), 3.28 (s, 2H), 3.04 (s, 6H), 1.87 (d, J =

13.0 Hz, 2H), 1.79 (dq, *J* = 10.6, 6.5, 5.2 Hz, 1H), 1.57 – 1.41 (m, 2H), 1.04 (d, *J* = 6.3 Hz, 3H) ppm. ^{13}C NMR (101 MHz, DMSO-d_6) δ 159.61, 154.97, 152.42, 144.74, 141.27, 133.84, 131.09, 126.85, 126.30, 123.09, 120.32, 119.49, 113.70, 112.21, 104.69, 52.51, 38.31, 34.02, 30.50, 21.98 ppm. HRMS *m/z*: calcd for $C_{26}H_{32}N_3^+$, $[M-I]^+$ = 386.25907, found 386.25995. HPLC analysis: retention time at 2.833 min (MeOH/H_2O = 50:50 v/v), purity 96.8%.

4.3.4 (*E*)-2-(4-(dimethylamino)styryl)-1-methyl-4-(pyrrolidin-1-yl)quinolin-1-ium (A4).

Orange solid with yield 90.4%; Melting point: 298.6-300.5 ℃; ^{1}H NMR (400 MHz, DMSO-d_6) δ 8.49 (d, *J* = 8.6 Hz, 1H), 8.13 (d, *J* = 8.9 Hz, 1H), 7.97 (t, *J* = 7.2 Hz, 1H), 7.72 (d, *J* = 9.2 Hz, 1H), 7.69 (d, *J* = 2.3 Hz, 2H), 7.64 (t, *J* = 7.7 Hz, 1H), 7.31 (d, *J* = 15.7 Hz, 1H), 6.97 (s, 1H), 6.79 (d, *J* = 9.0 Hz, 2H), 4.08 (s, 3H), 4.00 (s, 4H), 3.02 (s, 6H), 2.06 (s, 4H) ppm. ^{13}C NMR (101 MHz, DMSO-d_6) δ 154.51, 153.31, 152.08, 142.60, 141.26, 133.57, 130.53, 127.54, 125.12, 123.19, 118.73, 118.61, 114.57, 112.23, 99.76, 53.77, 38.04 ppm. HRMS *m/z*: calcd for $C_{24}H_{28}N_3^+$, $[M-I]^+$ = 358.22777, found 358.22794. HPLC analysis: retention time at 2.873 min (MeOH/H_2O = 50:50 v/v), purity 95.4%.

4.3.5 (*E*)-2-(4-(dimethylamino)styryl)-1-methyl-4-(propylamino)quinolin-1-ium (A5).

Reddish brown solid with yield 88.3%; Melting point: 277.1-280.6 ℃; ^{1}H NMR (400 MHz, DMSO-d_6) δ 8.84 (d, *J* = 5.5 Hz, 1H), 8.52 (d, *J* = 8.4 Hz, 1H), 8.15 (d, *J* = 10.0 Hz, 1H), 7.98 (t, *J* = 7.3 Hz, 1H), 7.73 (d, *J* = 6.6 Hz, 2H), 7.70 (s, 2H), 7.33 (d, *J* = 15.7 Hz, 1H), 7.04 (s, 1H), 6.78 (d, *J* = 9.0 Hz, 2H), 4.09 (s, 3H), 3.60 (q, *J* = 6.6 Hz, 2H), 3.02 (s, 6H), 1.78 (q, *J* = 7.3 Hz, 2H), 1.02 (t, *J* = 7.4 Hz, 3H) ppm. ^{13}C NMR (101 MHz, DMSO-d_6) δ 155.33, 153.73, 152.12, 143.29, 139.99, 134.00, 130.66, 126.33, 123.70, 123.15, 119.24, 117.70, 114.57, 112.17, 96.40, 45.06, 37.79, 21.71, 11.95 ppm. HRMS *m/z*: calcd for $C_{23}H_{28}N_3^+$, $[M-I]^+$ = 346.22777, found 346.22823. HPLC analysis: retention time at 2.907 min (MeOH/H_2O = 50:50 v/v), purity 95.1%.

4.3.6 (*E*)-4-(butylamino)-2-(4-(dimethylamino)styryl)-1-methylquinolin-1-ium (A6).

Brown solid with yield 87.8%; Melting point: 259.7-263.4 ℃; ^{1}H NMR (400 MHz, DMSO-d_6) δ 8.81 (s, 1H), 8.51 (d, *J* = 7.0 Hz, 1H), 8.16 (d, *J* = 8.9 Hz, 1H), 7.98 (t, *J* = 7.9 Hz, 1H), 7.73 (s, 1H), 7.71 (d, *J* = 6.8 Hz, 3H), 7.34 (d, *J* = 15.8 Hz, 1H), 7.05 (s, 1H), 6.79 (d, *J* = 8.9 Hz, 2H), 4.09 (s, 3H), 3.63 (q, *J* = 6.5 Hz, 2H), 3.02 (s, 6H), 1.78 – 1.69 (m, 2H), 1.49 – 1.41 (m, 2H), 0.97 (t, *J* = 7.4 Hz, 3H) ppm. ^{13}C NMR (101 MHz, DMSO-d_6) δ 155.33, 153.68, 152.14, 143.29, 139.99,

134.01, 130.66, 126.33, 123.71, 123.14, 119.25, 117.72, 114.60, 112.19, 96.39, 43.19, 37.78, 30.42, 20.19, 14.26 ppm. HRMS *m/z*: calcd for $C_{24}H_{30}N_3^+$, $[M-I]^+$ = 360.24342, found 360.24352. HPLC analysis: retention time at 2.825 min (MeOH/H_2O = 50:50 v/v), purity 97.4%.

4.3.7 (*E*)-2-(4-(dimethylamino)styryl)-1-methyl-4-(pentylamino)quinolin-1-ium (A7).

Orange solid with yield 86.2%; Melting point: 231.2-236.6 ℃; ^{1}H NMR (400 MHz, DMSO-d_6) δ 8.83 (t, *J* = 5.6 Hz, 1H), 8.51 (d, *J* = 8.5 Hz, 1H), 8.17 (d, *J* = 8.8 Hz, 1H), 7.99 (t, *J* = 7.3 Hz, 1H), 7.75 – 7.68 (m, 4H), 7.35 (d, *J* = 15.8 Hz, 1H), 7.05 (s, 1H), 6.80 (d, *J* = 9.0 Hz, 2H), 4.10 (s, 3H), 3.63 (q, *J* = 6.6 Hz, 2H), 3.03 (s, 6H), 1.76 (t, *J* = 7.2 Hz, 2H), 1.40 (dt, *J* = 8.7, 4.7 Hz, 4H), 0.91 (t, *J* = 6.9 Hz, 3H) ppm. ^{13}C NMR (101 MHz, DMSO-d_6) δ 155.32, 153.65, 152.13, 143.28, 139.98, 134.00, 130.66, 126.33, 123.71, 123.14, 119.24, 117.71, 114.59, 112.19, 96.38, 43.44, 37.79, 29.15, 28.00, 22.37, 14.41 ppm. HRMS *m/z*: calcd for $C_{25}H_{32}N_3^+$, $[M-I]^+$ = 374.25907, found 374.25902. HPLC analysis: retention time at 2.865 min (MeOH/H_2O = 50:50 v/v), purity 95.6%.

4.3.8 (*E*)-2-(4-(dimethylamino)styryl)-1-methyl-4-((3-phenylpropyl)amino)quinolin-1-ium (A8).

Orange solid with yield 89.7%; Melting point: 287.9-293.3 ℃; ^{1}H NMR (400 MHz, DMSO-d_6) δ 8.87 (t, *J* = 5.7 Hz, 1H), 8.50 (d, *J* = 7.1 Hz, 1H), 8.17 (d, *J* = 8.8 Hz, 1H), 7.99 (t, *J* = 7.9 Hz, 1H), 7.71 (d, *J* = 8.9 Hz, 3H), 7.66 (d, *J* = 15.6 Hz, 1H), 7.34 (d, *J* = 15.7 Hz, 1H), 7.29 (s, 2H), 7.28 (s, 2H), 7.18 (ddd, *J* = 8.7, 6.0, 2.9 Hz, 1H), 7.00 (s, 1H), 6.81 (d, *J* = 9.0 Hz, 2H), 4.10 (s, 3H), 3.66 (q, *J* = 6.6 Hz, 2H), 3.04 (s, 6H), 2.80 – 2.75 (m, 2H), 2.10 – 2.04 (m, 2H) ppm. ^{13}C NMR (101 MHz, DMSO-d_6) δ 155.39, 153.72, 152.17, 143.30, 141.87, 140.01, 134.04, 130.68, 128.85, 128.79, 126.39, 123.73, 123.12, 119.26, 117.77, 114.62, 112.22, 100.00, 96.39, 43.03, 37.78, 32.93, 29.98 ppm. HRMS *m/z*: calcd for $C_{29}H_{32}N_3^+$, $[M-I]^+$ = 422.25907, found 422.25900. HPLC analysis: retention time at 2.887 min (MeOH/H_2O = 50:50 v/v), purity 95.7%.

4.3.9 (*E*)-2-(4-(dimethylamino)styryl)-4-((3-hydroxypropyl)amino)-1-methylquinolin-1-ium (A9).

Tangerine solid with yield 84.1%; Melting point: 279.4-282.5 ℃; ^{1}H NMR (400 MHz, DMSO-d_6) δ 8.87 (t, *J* = 5.7 Hz, 1H), 8.48 (d, *J* = 7.1 Hz, 1H), 8.17 (d, *J* = 8.9 Hz, 1H), 7.99 (t, *J* = 7.3 Hz, 1H), 7.72 (t, *J* = 8.8 Hz, 4H), 7.35 (d, *J* = 15.7 Hz, 1H), 7.10 (s, 1H), 6.79 (d, *J* = 8.9 Hz, 2H), 4.75 (t, *J* = 5.0 Hz, 1H), 4.10 (s, 3H), 3.69 (q, *J* = 6.6 Hz, 2H), 3.59 (q, *J* = 5.7 Hz, 2H), 3.03 (s, 6H),

1.91 (t, J = 6.5 Hz, 2H) ppm. ^{13}C NMR (101 MHz, DMSO-d_6) δ 155.28, 153.70, 152.12, 143.27, 139.96, 133.98, 130.66, 126.34, 123.63, 123.12, 119.24, 117.72, 114.56, 112.17, 96.37, 58.65, 37.76, 31.61 ppm. HRMS *m/z*: calcd for $C_{23}H_{28}N_3O^+$, $[M-I]^+$ = 362.22269, found 362.22269. HPLC analysis: retention time at 2.937 min (MeOH/H_2O = 50:50 v/v), purity 95.1%.

4.3.10 (*E*)-2-(4-(dimethylamino)styryl)-1-methylquinolin-1-ium (A10).

Dark brown solid with yield 87.5%; Melting point: 272.4-277.8 ℃; ^{1}H NMR (400 MHz, DMSO-d_6) δ 8.80 (d, J = 9.1 Hz, 1H), 8.50 (d, J = 9.2 Hz, 1H), 8.42 (d, J = 9.0 Hz, 1H), 8.26 (d, J = 9.4 Hz, 1H), 8.23 (s, 1H), 8.08 (ddd, J = 8.8, 7.1, 1.6 Hz, 1H), 7.85 (d, J = 8.9 Hz, 3H), 7.54 (d, J = 15.5 Hz, 1H), 6.81 (d, J = 9.1 Hz, 2H), 4.44 (s, 3H), 3.07 (s, 6H) ppm. ^{13}C NMR (101 MHz, DMSO-d_6) δ 156.79, 153.32, 149.39, 142.33, 139.67, 134.60, 132.46, 130.26, 128.48, 127.27, 122.87, 120.68, 119.30, 112.31 ppm. HRMS *m/z*: calcd for $C_{20}H_{21}N_2^+$, $[M-I]^+$ = 289.16993, found 289.17026. HPLC analysis: retention time at 2.865 min (MeOH/H_2O = 50:50 v/v), purity 95.3%.

4.3.11 (*E*)-4-(4-(dimethylamino)styryl)-1-methyl-2-morpholinoquinolin-1-ium (B1).

Dark green solid with yield 86.1%; Melting point: 245.4-248.2 ℃; ^{1}H NMR (400 MHz, DMSO-d_6) δ 8.73 (d, J = 8.3 Hz, 1H), 8.07 (d, J = 8.2 Hz, 1H), 8.03 (s, 1H), 7.98 (s, 1H), 7.86 – 7.79 (m, 3H), 7.78 – 7.72 (m, 2H), 6.82 (d, J = 8.6 Hz, 2H), 4.07 (s, 3H), 3.88 (s, 4H), 3.69 (s, 4H), 3.05 (s, 6H) ppm. ^{13}C NMR (101 MHz, DMSO-d_6) δ 158.99, 152.21, 151.16, 142.63, 140.61, 133.97, 130.94, 126.73, 126.15, 123.76, 122.90, 119.64, 114.20, 112.34, 108.83, 66.24, 51.48, 40.99 ppm. HRMS *m/z*: calcd for $C_{24}H_{28}N_3O^+$, $[M-I]^+$ = 374.22269, found 374.22235. HPLC analysis: retention time at 2.836 min (MeOH/H_2O = 50:50 v/v), purity 96.0%.

4.3.12 (*E*)-4-(4-(dimethylamino)styryl)-1-methyl-2-(piperidin-1-yl)quinolin-1-ium (B2).

Dark green solid with yield 82.7%; Melting point: 242.1-243.8 ℃; ^{1}H NMR (400 MHz, DMSO-d_6) δ 8.69 (d, J = 8.2 Hz, 1H), 8.02 (s, 1H), 8.01 (d, J = 2.7 Hz, 1H), 7.96 (d, J = 15.8 Hz, 1H), 7.83 – 7.78 (m, 3H), 7.76 – 7.71 (m, 2H), 6.81 (d, J = 8.9 Hz, 2H), 4.03 (s, 3H), 3.63 (s, 4H), 3.04 (s, 6H), 1.80 (s, 4H), 1.73 (s, 2H) ppm. ^{13}C NMR (101 MHz, DMSO-d_6) δ 159.52, 152.14, 150.71, 142.16, 140.64, 133.79, 130.82, 126.51, 126.08, 123.82, 122.72, 119.54, 114.37, 112.33, 109.11, 52.34, 44.24, 41.14, 25.77, 23.66, 22.69, 22.07 ppm. HRMS *m/z*: calcd for $C_{25}H_{30}N_3^+$, $[M-I]^+$ = 372.24342, found 372.24377. HPLC analysis: retention time at 2.796 min (MeOH/H_2O = 50:50 v/v), purity 99.1%.

4.3.13 (*E*)-4-(4-(dimethylamino)styryl)-1-methyl-2-(4-methylpiperidin-1-yl)quinolin-1-ium (B3).

Dark brown solid with yield 86.1%; Melting point: 209.5-213.9 ℃; ^{1}H NMR (400 MHz, DMSO-d_6) δ 8.69 (d, J = 8.1 Hz, 1H), 8.02 (s, 1H), 8.01 (d, J = 2.6 Hz, 1H), 7.96 (d, J = 15.7 Hz, 1H), 7.83 – 7.78 (m, 3H), 7.75 – 7.72 (m, 2H), 6.81 (d, J = 9.0 Hz, 2H), 4.03 (s, 3H), 3.63 (s, 4H), 3.04 (s, 6H), 1.80 (s, 5H), 1.74 (s, 3H) ppm. ^{13}C NMR (101 MHz, DMSO-d_6) δ 159.51, 152.12, 150.70, 142.15, 140.62, 133.78, 130.83, 126.50, 126.08, 123.82, 122.71, 119.54, 114.36, 112.32, 109.09, 52.35, 41.15, 25.78, 23.66 ppm. HRMS *m/z*: calcd for $C_{26}H_{32}N_3^+$, $[M\text{-}I]^+$ = 386.25907, found 386.25830. HPLC analysis: retention time at 2.829 min (MeOH/H_2O = 50:50 v/v), purity 96.6%.

4.3.14 (*E*)-4-(4-(dimethylamino)styryl)-1-methyl-2-(pyrrolidin-1-yl)quinolin-1-ium (B4).

Dark brown solid with yield 83.7%; Melting point: 247.7-250.2 ℃; ^{1}H NMR (400 MHz, DMSO-d_6) δ 8.55 (d, J = 7.9 Hz, 1H), 7.93 (s, 1H), 7.93 (d, J = 1.8 Hz, 1H), 7.83 (d, J = 15.8 Hz, 1H), 7.77 – 7.69 (m, 3H), 7.65 – 7.59 (m, 2H), 6.80 (d, J = 9.0 Hz, 2H), 3.99 (s, 3H), 3.91 (s, 4H), 3.03 (s, 6H), 2.03 (s, 4H) ppm. ^{13}C NMR (101 MHz, DMSO-d_6) δ 156.81, 151.89, 148.53, 140.90, 140.68, 133.13, 130.42, 125.86, 125.53, 123.91, 122.05, 118.46, 114.74, 112.34, 107.21, 53.18, 41.94, 25.91 ppm. HRMS *m/z*: calcd for $C_{24}H_{28}N_3^+$, $[M\text{-}I]^+$ = 358.22777, found 358.22765. HPLC analysis: retention time at 2.841 min (MeOH/H_2O = 50:50 v/v), purity 95.3%.

4.3.15 (*E*)-4-(4-(dimethylamino)styryl)-1-methyl-2-(propylamino)quinolin-1-ium (B5).

Dark brown solid with yield 88.7%; Melting point: 264.5-270.3 ℃; ^{1}H NMR (400 MHz, DMSO-d_6) δ 8.55 (d, J = 6.9 Hz, 2H), 8.01 (d, J = 7.8 Hz, 1H), 7.91 (t, J = 7.9 Hz, 1H), 7.78 (d, J = 15.8 Hz, 2H), 7.75 – 7.74 (m, 1H), 7.71 (d, J = 15.8 Hz, 1H), 7.61 (t, J = 7.1 Hz, 1H), 7.48 (s, 1H), 6.80 (d, J = 9.0 Hz, 2H), 3.90 (s, 3H), 3.68 (t, J = 7.1 Hz, 2H), 3.03 (s, 6H), 1.75 (q, J = 7.2 Hz, 2H), 1.02 (t, J = 7.4 Hz, 3H) ppm. ^{13}C NMR (101 MHz, DMSO-d_6) δ 153.22, 151.82, 149.45, 140.57, 138.99, 133.32, 130.37, 126.45, 125.21, 123.88, 121.19, 117.46, 114.89, 112.29, 103.53, 45.10, 35.26, 22.51, 11.66 ppm. HRMS *m/z*: calcd for $C_{23}H_{28}N_3^+$, $[M\text{-}I]^+$ = 346.22777, found 346.22806. HPLC analysis: retention time at 2.827 min (MeOH/H_2O = 50:50 v/v), purity 96.4%.

4.3.16 (*E*)-2-(butylamino)-4-(4-(dimethylamino)styryl)-1-methylquinolin-1-ium (B6).

Red solid with yield 89.1%; Melting point: 246.3-254.2 ℃; ^{1}H NMR (400 MHz, DMSO-d_6) δ

8.55 (d, J = 7.0 Hz, 2H), 8.01 (d, J = 8.0 Hz, 1H), 7.91 (t, J = 7.2 Hz, 1H), 7.78 (d, J = 15.6 Hz, 2H), 7.74 (s, 1H), 7.71 (d, J = 15.8 Hz, 1H), 7.61 (t, J = 7.6 Hz, 1H), 7.47 (s, 1H), 6.79 (d, J = 8.9 Hz, 2H), 3.89 (s, 3H), 3.11 (s, 2H), 3.02 (s, 6H), 1.71 (p, J = 7.2 Hz, 2H), 1.50 – 1.42 (m, 2H), 0.98 (t, J = 7.3 Hz, 3H) ppm. ^{13}C NMR (101 MHz, DMSO-d_6) δ 153.14, 151.82, 149.43, 140.55, 138.99, 133.31, 130.37, 126.44, 125.20, 123.87, 121.17, 117.45, 114.89, 112.29, 103.52, 45.42, 43.30, 35.31, 31.26, 24.10, 19.89, 14.25 ppm. HRMS *m/z*: calcd for $C_{24}H_{30}N_3^+$, $[M-I]^+$ = 360.24342, found 360.24354. HPLC analysis: retention time at 2.837 min (MeOH/H_2O = 50:50 v/v), purity 96.4%.

4.3.17 (*E*)-4-(4-(dimethylamino)styryl)-1-methyl-2-(pentylamino)quinolin-1-ium (B7).

Brown solid with yield 90.1%; Melting point: 203.7-208.1 ℃; ^{1}H NMR (400 MHz, DMSO-d_6) δ 8.55 (d, J = 6.7 Hz, 2H), 8.00 (d, J = 8.7 Hz, 1H), 7.90 (t, J = 7.2 Hz, 1H), 7.79 (s, 1H), 7.74 (d, J = 6.5 Hz, 2H), 7.70 (d, J = 15.8 Hz, 1H), 7.60 (t, J = 7.4 Hz, 1H), 7.46 (s, 1H), 6.79 (d, J = 8.3 Hz, 2H), 3.89 (s, 3H), 3.69 (q, J = 6.7 Hz, 2H), 3.02 (s, 6H), 1.72 (q, J = 7.2 Hz, 2H), 1.40 (tq, J = 12.8, 6.8 Hz, 4H), 0.92 (t, J = 6.8 Hz, 3H) ppm. ^{13}C NMR (101 MHz, DMSO-d_6) δ 153.16, 151.83, 149.45, 140.56, 139.00, 133.33, 130.36, 126.45, 125.21, 123.86, 121.18, 117.46, 114.91, 112.30, 103.53, 99.99, 43.51, 35.24, 28.80, 22.34, 14.39 ppm. HRMS *m/z*: calcd for $C_{25}H_{32}N_3^+$, $[M-I]^+$ = 374.25907, found 374.25801. HPLC analysis: retention time at 2.819 min (MeOH/H_2O = 50:50 v/v), purity 97.8%.

4.3.18 (*E*)-4-(4-(dimethylamino)styryl)-1-methyl-2-((3-phenylpropyl)amino)quinolin-1-ium (B8).

Red solid with yield 85.3%; Melting point: 188.9-195.6 ℃; ^{1}H NMR (400 MHz, DMSO-d_6) δ 8.62 – 8.50 (m, 2H), 8.00 (d, J = 8.7 Hz, 1H), 7.90 (t, J = 7.2 Hz, 1H), 7.75 (d, J = 8.7 Hz, 2H), 7.70 (s, 2H), 7.60 (t, J = 7.6 Hz, 1H), 7.42 (s, 1H), 7.28 (d, J = 4.4 Hz, 4H), 7.21 – 7.14 (m, 1H), 6.80 (d, J = 9.0 Hz, 2H), 3.87 (s, 3H), 3.73 (t, J = 7.1 Hz, 2H), 3.02 (s, 6H), 2.78 (t, J = 7.6 Hz, 2H), 2.04 (p, J = 7.2 Hz, 2H) ppm. ^{13}C NMR (101 MHz, DMSO-d_6) δ 153.18, 151.84, 149.48, 141.87, 140.55, 139.00, 133.34, 130.38, 128.83, 128.80, 126.46, 126.39, 125.22, 123.84, 121.21, 117.44, 114.93, 112.30, 103.49, 43.17, 35.20, 32.66, 30.78 ppm. HRMS *m/z*: calcd for $C_{29}H_{32}N_3^+$, $[M-I]^+$ = 422.25907, found 422.25857. HPLC analysis: retention time at 2.837 min (MeOH/H_2O = 50:50 v/v), purity 96.1%.

4.3.19 (*E*)-4-(4-(dimethylamino)styryl)-2-((3-hydroxypropyl)amino)-1-methylquinolin-1-

ium (B9).

Orange solid with yield 87.2%; Melting point: 234.3-237.8 ℃; ^{1}H NMR (400 MHz, DMSO-d_6) δ 8.56 (d, J = 8.4 Hz, 2H), 8.01 (d, J = 8.7 Hz, 1H), 7.91 (t, J = 7.2 Hz, 1H), 7.78 (d, J = 16.6 Hz, 2H), 7.73 (s, 2H), 7.61 (t, J = 7.6 Hz, 1H), 7.54 (s, 1H), 6.79 (d, J = 8.8 Hz, 2H), 4.80 (s, 1H), 3.89 (s, 3H), 3.76 (t, J = 6.9 Hz, 2H), 3.60 (q, J = 5.3 Hz, 2H), 3.02 (s, 6H), 1.88 (p, J = 6.5 Hz, 2H) ppm. ^{13}C NMR (101 MHz, DMSO-d_6) δ 153.24, 151.83, 149.39, 140.51, 138.97, 133.31, 130.37, 126.44, 125.20, 123.85, 121.19, 117.43, 114.88, 112.29, 103.54, 58.44, 35.12, 32.25 ppm. HRMS *m/z*: calcd for $C_{23}H_{28}N_3O^+$, $[M\text{-}I]^+$ = 362.22269, found 362.22243. HPLC analysis: retention time at 2.910 min (MeOH/H_2O = 50:50 v/v), purity 95.2%.

4.3.20 (*E*)-4-(4-(dimethylamino)styryl)-1-methylquinolin-1-ium (B10).

Dark green solid with yield 89.3%; Melting point: 288.7-293.3 ℃; ^{1}H NMR (400 MHz, DMSO-d_6) δ 9.12 (d, J = 6.7 Hz, 1H), 9.03 (d, J = 8.8 Hz, 1H), 8.35 (s, 1H), 8.33 (d, J = 1.6 Hz, 1H), 8.22 (d, J = 7.0 Hz, 1H), 8.18 (d, J = 11.8 Hz, 1H), 8.03 – 7.96 (m, 2H), 7.87 (d, J = 9.0 Hz, 2H), 6.83 (d, J = 9.0 Hz, 2H), 4.45 (s, 3H), 3.07 (s, 6H) ppm. ^{13}C NMR (101 MHz, DMSO-d_6) δ 153.64, 152.78, 147.25, 145.16, 139.26, 135.09, 131.82, 129.03, 126.83, 126.23, 123.53, 119.52, 114.42, 113.59, 112.38, 44.50 ppm. HRMS *m/z*: calcd for $C_{20}H_{21}N_2^+$, $[M\text{-}I]^+$ = 289.16993, found 289.17029. HPLC analysis: retention time at 2.803 min (MeOH/H_2O = 50:50 v/v), purity 95.2%.

4.4 Determination of the water solubility of 1-methylquinolinium-based derivatives A1-A10, B1-B10

The water solubility of the compounds was determined with the reported method [49]. Briefly, the standard solutions of compounds were prepared into five gradient concentrations using ultrapure water. The compound was completely dissolved in the solution. These standard solutions were analyzed with HPLC and the peak area of each concentration was recorded to obtain a linear regression equation: $Y = AX+B$. The results were listed in **Table S4**. The saturated solution of the compound was prepared by sonicating or oscillating overnight and then centrifuged for 20 min. The supernatant was diluted with ultrapure water and then was determined with HPLC. The water solubility was calculated by using the linear regression equations obtained. A Diamonsil C18 column (250 × 4.6 mm, 5 μm) was used at room temperature with an elution using the mobile phase (MeOH/H_2O = 50:50 v/v) and the wavelength selected for detection was 225 nm.

4.5 Minimum inhibitory concentration assay (MIC)

The minimum inhibitory concentrations (MICs) were assessed by broth micro-dilution method in 96-well microtiter plates in accordance with the Clinical and Laboratory Standard Institute (CLSI) guidelines [34]. The bacterial culture was diluted to a concentration of 5×10^5 CFU/mL using MHB (Mueller-Hinton broth) medium and transferred into 96-well microplates. The tested compounds were diluted by DMSO and then added into plates with a series of concentrations, in which the DMSO concentration was fixed at 1%. Ciprofloxacin, ampicillin, vancomycin, and rifampin were used as positive control and 1% DMSO was used as negative control. After incubation at 37 ℃ for 20-24 h, the minimum inhibitory concentrations were determined as the lowest concentration, which had no visibly growth of the tested bacteria. Three repeat assays were conducted for each test.

4.6 Minimum bactericidal concentration assay (MBC)

Based on the MIC assay described above, 100 μL of the MIC culture were spread onto the TSB agar plate and then incubated for 24 h at 37 ℃. MBC was defined as the minimum concentration of tested compounds that can make 3 orders of magnitude reduction of bacteria [50]. In the assay, MBC was equal to the lowest concentration that the colonies on the plate were less than 5.

4.7 Time-killing curve assay

A growth culture of *S. aureus* ATCC 29213 was diluted to 10^6 CFU/mL in MHB medium, and then various concentrations (0×, 1×, 2×, 4×, 8×MIC) of compounds were added. The cultures were incubated at 37 ℃ with shaking. Then, 100 μL of the sample were taken for serial dilution at specific time points ranging from 0-24 h and spread onto TSB agar plates. The agar plates after 18 h incubation, the bacterial counts were recorded.

4.8 Checkboard assay

The checkboard method was used to quantify synergy between compounds and methicillin against MRSA ATCC BAA-41 following the previous procedures [23, 48]. In the assay, MRSA ATCC BAA-41 was diluted to 5×10^5 CFU/mL bacterial culture. Methicillin was pre-diluted in the bacterial culture into 96-well microplates. Then, the compounds were diluted as well. The 96-well microtiter plates were incubated at 37 ℃ for 24 h. The $OD_{620\ nm}$ of the culture mixture were then

633 measured with a microplate reader. Fractional inhibitory concentration (FIC) = MIC in combination
634 / MIC alone; FIC index = $FIC_{compound} + FIC_{methicillin}$.

635 Polymyxin B nonapeptide (PMBN) was used to determine the antibacterial activity of
636 compounds against Gram-negative bacteria [51]. The procedures were followed the checkboard
637 method as described above, with the difference that the concentration of PMBN was 20 μg/mL in
638 each well.

639 **4.9 Visualization of bacterial morphology**

640 *B. subtilis* CMCC (B) 63501 and *S. aureus* ATCC 29213 were activated and incubated in LB
641 medium. Then the bacterial cells were diluted to 1×10^5 CFU/mL and mixed with absence or various
642 concentrations of tested compounds. After shaking at 37 ℃ for 4 h, the cells were collected and re-
643 suspended in phosphate buffer solution. Then, 3 μL of bacterial suspension were added onto the
644 microscope slide pre-treated with 0.1% (w/v) poly-L-lysine. The morphology of *B. subtilis* and *S.*
645 *aureus* was observed at a 400× magnification. The images were captured using Olympus IX71
646 microscope and ZEISS LSM 800 with Airscan microscope.

647 **4.10 Polymerization assay**

648 *S. aureus* FtsZ protein was cloned and overexpressed according to the previous report [14].
649 The polymerization assay was carried out with a microplate reader since the polymerization of FtsZ
650 was proportional to $A_{340\ nm}$ [52]. *S. aureus* FtsZ (6 μM) in 50 mM MOPS buffer (pH 6.5) were pre-
651 incubated with 1% DMSO (vehicle) or various concentrations of tested compounds at 25 ℃. Then,
652 50 mM KCl, 2 mM $MgCl_2$ and 1 mM $CaCl_2$ were added for baseline establishment. After 10 min
653 scanning, a final concentration of 1 mM GTP was added and monitored the signal of $A_{340\ nm}$ for
654 another 2000 s. All the polymerization data were processed by the corresponding background
655 subtraction and repeated three times.

656 **4.11 GTPase activity assay**

657 The effect of the tested compounds on the GTPase activity of *S. aureus* FtsZ were measured
658 in 96-well microplates using the ATPase/GTPase Activity Assay Kit (Sigma-Aldrich, MAK113)
659 according to the kit's protocol and optimized conditions. *S. aureus* FtsZ proteins (5 μM) were
660 incubated with 1% DMSO or compounds (0.5, 1, 2, 4, 8, 16, 32, 64 μg/mL) for 30 min at 25 ℃.
661 Then, 1 mM GTP were added into each well and incubated at 25 ℃. After 30 min, 200 μL reagent

buffer were added to terminate the GTPase reaction and incubated for another 30 minutes. The absorbance at 620 nm was read to measure the concentration of inorganic phosphate.

4.12 Circular dichroism assay

S. aureus FtsZ (20 μM) was incubated without or with tested compounds at different concentrations (2, 4, 8 μg/mL) in 20 mM Tris-HCl (pH 7.4) for 30 min at 25 ℃. The CD spectra were monitored by a Chirascan spectrophotometer (Applied Photophysics Ltd.) over a wavelength range of 190-260 nm with a 0.5 mm path length quartz cuvette and 1 nm bandwidth. Each spectrum recorded was an average of three scans. Chirascan Pro-Data Viewer and CDNN software were used for data plotting and deconvolution analysis, respectively.

4.13 Fluorescence titration assay

The fluorescence titration assay was conducted according to the method described previously [35]. *S. aureus* FtsZ proteins were added into 20 mM Tris-HCl (pH 7.4) buffer containing 5 μM compound with a gradient concentration. After the addition of FtsZ protein, the mixture was incubated at 25 ℃ for 2 minutes. The fluorescence spectra were recorded using LS-55 fluorescence spectrometer (Perkin Elmer) from 400-800 nm. The slit width and scan speed were set at 10 nm and 800 nm/min, respectively.

4.14 Isothermal titration calorimetry (ITC) assay

ITC measurements were performed on MicroCal PEAQ-ITC (Malvern Panalytical). *S. aureus* FtsZ proteins (10 μM) and the tested compound (100 μM) were dialyzed against PBS buffer, and then loaded into a sample cell and an injection syringe, respectively. The titration contained 19 injections of the tested compounds at 25 ℃ (0.4 μL for the first injection, 2 μL for the rest injections), with 150-second spacing between each injection. The experimental data were processed by the built-in analysis software of the instrument.

4.15 Molecular docking study

The molecular docking procedures were performed using Discovery Studio version 2016 (DS 2016). The X-ray crystal structure of *S. aureus* FtsZ (PDB ID: 4DXD, with PC190723 and GDP) was downloaded from RCSB PDB database. Water molecules and co-crystal ligands were removed, and the protein was prepared using DS automated procedures. The structures of **A3** and **B3** were converted into 3D and minimized using DS small molecule tool. The docking studies were

implemented using DS-CDocker protocol. The docking results were analyzed and visually inspected in DS 2016.

4.16 Hemolytic activity assay

In this experiment, red blood cells (RBC) from Kunming mice were used to test the hemolytic activity of the compounds by following the previously described procedures. The RBC were washed with PBS to prepare 2% RBC suspension, and a series of concentrations of compounds were prepared in PBS, then mixed with a volume ratio of 1:1. After incubation for 1 h, the mixtures were centrifuged at 10000 rpm for 5 min, and then supernatant were taken to measure the absorbance at 540 nm. Water and Triton X-100 were used as positive control and PBS was used as negative control. Hemolysis was considered to occur when the rate was >5% [53].

4.17 MTT assay

Mouse fibroblasts (L929) cells and human renal tubular (HK-2) cells were used to evaluate the cytotoxic of compounds by MTT assay. After resuscitation, the cells were collected and diluted to 5000 cells/mL approximately. Then, 100 μL of cell suspensions were seeded into a 96-well microplate and incubated for 24 h. The cells were then treated with the compound at different concentrations for 48 h and then 100 μL MTT (0.5 mg/mL) were added into every well for another 4 h incubation. After that, the absorbance was measured by microplate reader at 570 nm. In the assay, the culture medium was DMEM containing 10% FBS and 0.5% 100× Penicillin-Streptomycin solution. The cultivation condition was 37 ℃ and 5% CO_2.

4.18 Drug resistance assay

To investigate the drug resistance of compounds and the chosen antibiotics (vancomycin, ciprofloxacin, and rifampin) against *S. aureus* ATCC 29213 or *B. subtilis* CMCC (B) 63501, 35 passages of MIC measurements were performed referring to the previous method [54, 55]. The MIC values of first day were determined according to the method described in Section 4.5. The cells that incubated in sub-MIC well were diluted to approximately 5×10^5 CFU/mL for the next MIC measurement. The MIC values were recorded after 24 h incubation at 37 ℃. The MIC assays were repeated 35 passages with biological replicates.

Declaration of competing interest

The authors declare that they have no competing financial interests or personal relationships that could have appeared to influence the work reported in this paper.

Acknowledgements

This work was supported by the National Natural Science Foundation of China (81703333, 22077020 and 32050410289), Natural Science Foundation of Guangdong Province, China (2020A1515011326, 2017A030313078), Health and Medical Research Fund (HMRF) of the Food and Health Bureau, Hong Kong SAR (19200231), and PolyU Start-up Fund (P0035712]. We also acknowledge the supports received from Foshan Science and Technology Innovation Project (2020001004656) and Foshan Key Technology Project (1920001000262).

References

[1] S. Bassetti, S. Tschudin-Sutter, A. Egli, M. Osthoff, Optimizing antibiotic therapies to reduce the risk of bacterial resistance, Eur. J. Intern. Med. (2022).

[2] Z. Jian, L. Zeng, T. Xu, S. Sun, S. Yan, L. Yang, Y. Huang, J. Jia, T. Dou, Antibiotic resistance genes in bacteria: Occurrence, spread, and control, J. Basic. Microb. 61 (2021) 1049-1070.

[3] M.F. Varela, J. Stephen, M. Lekshmi, M. Ojha, N. Wenzel, L.M. Sanford, A.J. Hernandez, A. Parvathi, S.H. Kumar, Bacterial resistance to antimicrobial agents, Antibiotics 10 (2021) 593.

[4] M. Hailemariam, T. Alemayehu, B. Tadesse, N. Nigussie, A. Agegnehu, T. Habtemariam, M. Ali, E. Mitiku, E. Azerefegne, Major bacterial isolate and antibiotic resistance from routine clinical samples in Southern Ethiopia, Sci. Rep. 11 (2021) 1-9.

[5] N. Theriault, G. Tillotson, C.E. Sandrock, Global travel and Gram-negative bacterial resistance; implications on clinical management, Expert. Rev. Anti-infe. 19 (2021) 181-196.

[6] J. Wang, M.F. Ansari, C.-H. Zhou, Identification of unique quinazolone thiazoles as novel structural scaffolds for potential Gram-negative bacterial conquerors, J. Med. Chem. 64 (2021) 7630-7645.

[7] O. McNeilly, R. Mann, M. Hamidian, C. Gunawan, Emerging concern for silver nanoparticle resistance in Acinetobacter baumannii and other bacteria, Front. Microbiol. 12 (2021).

749 [8] R.L. Lock, E.J. Harry, Cell-division inhibitors: new insights for future antibiotics, Nat. Rev.
750 Drug. Discov. 7 (2008) 324-338.
751 [9] T. Den Blaauwen, J.M. Andreu, O. Monasterio, Bacterial cell division proteins as antibiotic
752 targets, Bioorg. Chem. 55 (2014) 27-38.
753 [10] K. Haranahalli, S. Tong, I. Ojima, Recent advances in the discovery and development of
754 antibacterial agents targeting the cell-division protein FtsZ, Bioorg. Med. Chem. 24 (2016) 6354-
755 6369.
756 [11] X. Li, S. Ma, Advances in the discovery of novel antimicrobials targeting the assembly of
757 bacterial cell division protein FtsZ, Eur. J. Med. Chem. 95 (2015) 1-15.
758 [12] K.D. Kusuma, M. Payne, A.T. Ung, A.L. Bottomley, E.J. Harry, FtsZ as an antibacterial target:
759 status and guidelines for progressing this avenue, ACS Infect. Dis. 5 (2019) 1279-1294.
760 [13] A. Casiraghi, L. Suigo, E. Valoti, V. Straniero, Targeting bacterial cell division: A binding site-
761 centered approach to the most promising inhibitors of the essential protein FtsZ, Antibiotics 9 (2020)
762 69.
763 [14] T.K. Beuria, M.K. Santra, D. Panda, Sanguinarine blocks cytokinesis in bacteria by inhibiting
764 FtsZ assembly and bundling, Biochemistry 44 (2005) 16584-16593.
765 [15] P.N. Domadia, A. Bhunia, J. Sivaraman, S. Swarup, D. Dasgupta, Berberine targets assembly
766 of Escherichia coli cell division protein FtsZ, Biochemistry 47 (2008) 3225-3234.
767 [16] N. Sun, F.Y. Chan, Y.J. Lu, M.A. Neves, H.K. Lui, Y. Wang, K.Y. Chow, K.F. Chan, S.C. Yan,
768 Y.C. Leung, R. Abagyan, T.H. Chan, K.Y. Wong, Rational design of berberine-based FtsZ inhibitors
769 with broad-spectrum antibacterial activity, PloS One 9 (2014) e97514.
770 [17] P. Domadia, S. Swarup, A. Bhunia, J. Sivaraman, D. Dasgupta, Inhibition of bacterial cell
771 division protein FtsZ by cinnamaldehyde, Biochem. Pharmacol. 74 (2007) 831-840.
772 [18] D.J. Haydon, N.R. Stokes, R. Ure, G. Galbraith, J.M. Bennett, D.R. Brown, P.J. Baker, V.V.
773 Barynin, D.W. Rice, S.E. Sedelnikova, J.R. Heal, J.M. Sheridan, S.T. Aiwale, P.K. Chauhan, A.
774 Srivastava, A. Taneja, I. Collins, J. Errington, L.G. Czaplewski, An inhibitor of FtsZ with potent
775 and selective anti-staphylococcal activity, Science 321 (2008) 1673-1675.
776 [19] M. Kaul, L. Mark, Y. Zhang, A.K. Parhi, Y.L. Lyu, J. Pawlak, S. Saravolatz, L.D. Saravolatz,
777 M.P. Weinstein, E.J. LaVoie, D.S. Pilch, TXA709, an FtsZ-targeting benzamide prodrug with

778 improved pharmacokinetics and enhanced in vivo efficacy against methicillin-resistant
779 Staphylococcus aureus, Antimicrob. Agents. Ch. 59 (2015) 4845-4855.
780 [20] G.M. Nepomuceno, K.M. Chan, V. Huynh, K.S. Martin, J.T. Moore, T.E. O'Brien, L.A. Pollo,
781 F.J. Sarabia, C. Tadeus, Z. Yao, D.E. Anderson, J.B. Ames, J.T. Shaw, Synthesis and evaluation of
782 quinazolines as inhibitors of the bacterial cell division protein FtsZ, ACS Med. Chem. Lett. 6 (2015)
783 308-312.
784 [21] TAXIS Pharmaceuticals, World Health Organization Names TAXIS' TXA709 as One of Only
785 2 (out of 26) Antibacterials Meeting All Innovation Criteria.
786 https://www.taxispharma.com/news/world-health-organization-who-names-txa709-as-one-of-
787 only-2-out-of-26-antibacterials-meeting-all-innovation-criteria/, 2021 (accessed 15 March 2022).
788 [22] TAXIS Pharmaceuticals, TAXIS Pharmaceuticals appears in June special issue on Antibiotics
789 in ACS Infectious Diseases. https://www.taxispharma.com/news/taxis-pharmaceuticals-appears-
790 in-june-special-issue-on-antibiotics-in-acs-infectious-diseases/, 2020 (accessed 15 March 2022).
791 [23] M. Kaul, L. Mark, A.K. Parhi, E.J. LaVoie, D.S. Pilch, Combining the FtsZ-targeting prodrug
792 TXA709 and the cephalosporin cefdinir confers synergy and reduces the frequency of resistance in
793 methicillin-resistant Staphylococcus aureus, Antimicrob. Agents. Ch. 60 (2016) 4290-4296.
794 [24] M. Henary, C. Kananda, L. Rotolo, B. Savino, E.A. Owens, G. Cravotto, Benefits and
795 applications of microwave-assisted synthesis of nitrogen containing heterocycles in medicinal
796 chemistry, RSC Adv. 10 (2020) 14170-14197.
797 [25] N. Kerru, L. Gummidi, S. Maddila, K.K. Gangu, S.B. Jonnalagadda, A review on recent
798 advances in nitrogen-containing molecules and their biological applications, Molecules 25 (2020)
799 1909.
800 [26] S. Cai, W. Yuan, Y. Li, X. Huang, Q. Guo, Z. Tang, Z. Fang, H. Lin, W.L. Wong, K.Y. Wong,
801 Y.J. Lu, N. Sun, Antibacterial activity of indolyl-quinolinium derivatives and study their mode of
802 action, Bioorg. Med. Chem. 27 (2019) 1274-1282.
803 [27] N. Sun, M. Li, S. Cai, Y. Li, C. Chen, Y. Zheng, X. Li, Z. Fang, H. Lv, Y.J. Lu, Antibacterial
804 evaluation and mode of action study of BIMQ, a novel bacterial cell division inhibitor, Biochem.
805 Bioph. Res. Co. 514 (2019) 1224-1230.
806 [28] S. Lin, H. Li, Y. Tao, J. Liu, W. Yuan, Y. Chen, Y. Liu, S. Liu, *In vitro* and *in vivo* evaluation

807 of membrane-active flavone amphiphiles: semisynthetic kaempferol-derived antimicrobials against
808 drug-resistant gram-positive bacteria, J. Med. Chem. 63 (2020) 5797-5815.
809 [29] B.X. Zheng, W. Long, Y.H. Zhang, X.H. Huang, C.C. Chen, D.X. Zhong, M.T. She, Z.X. Chen,
810 D.P. Cai, Y.J. Lu, W.L. Wong, Rational design of Red fluorescent and selective G-quadruplex DNA
811 sensing probes: The study of interaction signaling and the molecular structural relationship
812 achieving high specificity, Sensor. Actuat. B-chem. 314 (2020) 128075.
813 [30] M. Rbaa, S. Jabli, Y. Lakhrissi, M. Ouhssine, F. Almalki, T.B. Hadda, S. Messgo-Moumene,
814 A. Zarrouk, B. Lakhrissi, Synthesis, antibacterial properties and bioinformatics computational
815 analyses of novel 8-hydroxyquinoline derivatives, Heliyon 5 (2019) e02689.
816 [31] M. Vaara, Polymyxin derivatives that sensitize Gram-negative bacteria to other antibiotics,
817 Molecules 24 (2019) 249.
818 [32] R.A. Dixon, I. Chopra, Polymyxin B and polymyxin B nonapeptide alter cytoplasmic
819 membrane permeability in Escherichia coli, J. Antimicrob. Chemoth. 18 (1986) 557-563.
820 [33] H. Tsubery, I. Ofek, S. Cohen, M. Fridkin, Structure− function studies of polymyxin B
821 nonapeptide: implications to sensitization of gram-negative bacteria, J. Med. Chem. 43 (2000)
822 3085-3092.
823 [34] M.A. Wikler, J.F. Hindler, F.R. Cookerill, J.B. Patel, K. Bush, M. Powell, Methods for Dilution
824 Antimicrobial Sucseptibility tests for Bacteria that Grow Aerobically, M07-A08, Clinical and
825 Laboratory Standards Institute, 2009.
826 [35] Y. Li, N. Sun, H.L. Ser, W. Long, Y. Li, C. Chen, B. Zheng, X. Huang, Z. Liu, Y.J. Lu,
827 Antibacterial activity evaluation and mode of action study of novel thiazole-quinolinium
828 derivatives, RSC Adv. 10 (2020) 15000-15014.
829 [36] I. Odenholt, E. Löwdin, O. Cars, *In vitro* studies of the pharmacodynamics of teicoplanin
830 against Staphylococcus aureus, Staphylococcus epidermidis and Enterococcus faecium, Clin.
831 Microbiol. Infec. 9 (2003) 930-937.
832 [37] T.M. Cook, K.G. Brown, J.V. Boyle, W.A. Goss, Bactericidal action of nalidixic acid on
833 Bacillus subtilis, J. Bacteriol. 92 (1966) 1510-1514.
834 [38] N. Zhang, D. Song, W. Chen, S. Zhang, P. Zhang, N. Zhang, S. Ma, Modification of 5-
835 methylphenanthridium from benzothiazoles to indoles as potent FtsZ inhibitors: Broadening the

836 antibacterial spectrum toward vancomycin-resistant enterococci, Eur. J. Med. Chem. 224 (2021)
837 113723.
838 [39] Y.Y. Zheng, R.L. Du, S.Y. Cai, Z.H. Liu, Z.Y. Fang, T. Liu, L.Y. So, Y.J. Lu, N. Sun, K.Y.
839 Wong, Study of Benzofuroquinolinium Derivatives as a New Class of Potent Antibacterial Agent
840 and the Mode of Inhibition Targeting FtsZ, Front. Microbiol. 9 (2018).
841 [40] T.K. Beuria, P. Singh, A. Surolia, D. Panda, Promoting assembly and bundling of FtsZ as a
842 strategy to inhibit bacterial cell division: a new approach for developing novel antibacterial drugs,
843 Biochem. J. 423 (2009) 61-69.
844 [41] M. Kaul, Y. Zhang, A.K. Parhi, E.J. LaVoie, D.S. Pilch, Inhibition of RND-type efflux pumps
845 confers the FtsZ-directed prodrug TXY436 with activity against Gram-negative bacteria, Biochem.
846 Pharmacol. 89 (2014) 321-328.
847 [42] H.K. Lui, W. Gao, K.C. Cheung, W.B. Jin, N. Sun, J.W. Kan, I.L. Wong, J. Chiou, D. Lin, E.W.
848 Chan, Y.C. Leung, T.H. Chan, S. Chen, K.F. Chan, K.Y. Wong, Boosting the efficacy of anti-MRSA
849 β-lactam antibiotics via an easily accessible, non-cytotoxic and orally bioavailable FtsZ inhibitor,
850 Eur. J. Med. Chem. 163 (2019) 95-115.
851 [43] D. Rai, J.K. Singh, N. Roy, D. Panda, Curcumin inhibits FtsZ assembly: an attractive
852 mechanism for its antibacterial activity, Biochem. J. 410 (2008) 147-155.
853 [44] X. Xie, B. Choi, E. Largy, R. Guillot, A. Granzhan, M.P. Teulade-Fichou, Asymmetric
854 distyrylpyridinium dyes as red-emitting fluorescent probes for quadruplex DNA, Chem. Eur. J. 19
855 (2013) 1214-1226.
856 [45] F.H. Stootman, D.M. Fisher, A. Rodger, J.R. Aldrich-Wright, Improved curve fitting
857 procedures to determine equilibrium binding constants, Analyst 131 (2006) 1145-1151.
858 [46] P. Sass, H. Brötz-Oesterhelt, Bacterial cell division as a target for new antibiotics, Curr. Opin.
859 Microbiol. 16 (2013) 522-530.
860 [47] R.F. de Freitas, M. Schapira, A systematic analysis of atomic protein–ligand interactions in the
861 PDB, MedChemComm 8 (2017) 1970-1981.
862 [48] C.M. Tan, A.G. Therien, J. Lu, S.H. Lee, A. Caron, C.J. Gill, C. Lebeau-Jacob, L. Benton-
863 Perdomo, J.M. Monteiro, P.M. Pereira, N.L. Elsen, J. Wu, K. Deschamps, M. Petcu, S. Wong, E.
864 Daigneault, S. Kramer, L. Liang, E. Maxwell, D. Claveau, J. Vaillancourt, K. Skorey, J. Tam, H.

865 Wang, T.C. Meredith, S. Sillaots, L. Wang-Jarantow, Y. Ramtohul, E. Langlois, F. Landry, J.C. Reid,
866 G. Parthasarathy, S. Sharma, A. Baryshnikova, K.J. Lumb, M.G. Pinho, S.M. Soisson, T. Roemer,
867 Restoring methicillin-resistant Staphylococcus aureus susceptibility to β-lactam antibiotics, Sci.
868 Transl. Med. 4 (2012) 126-135.
869 [49] W. Long, B.X. Zheng, Y. Li, X.H. Huang, D.M. Lin, C.C. Chen, J.Q. Hou, T.M. Ou, W.L.
870 Wong, K. Zhang, Y.J. Lu, Rational design of small-molecules to recognize G-quadruplexes of c-
871 MYC promoter and telomere and the evaluation of their *in vivo* antitumor activity against breast
872 cancer, Nucleic. Acids. Res. 50 (2022) 1829-1848.
873 [50] F.R. Dias, J.S. Novais, T.A.d.N.S. Devillart, W.A. da Silva, M.O. Ferreira, R.d.S. Loureiro,
874 V.R. Campos, V.F. Ferreira, M.C. de Souza, H.C. Castro, A.C. Cunha, Synthesis and antimicrobial
875 evaluation of amino sugar-based naphthoquinones and isoquinoline-5, 8-diones and their
876 halogenated compounds, Eur. J. Med. Chem. 156 (2018) 1-12.
877 [51] R.L. Du, N. Sun, Y.H. Fung, Y.Y. Zheng, Y.W. Chen, P.H. Chan, W.L. Wong, K.Y. Wong,
878 Discovery of FtsZ inhibitors by virtual screening as antibacterial agents and study of the inhibition
879 mechanism, RSC Med. Chem. 13 (2022) 79-89.
880 [52] M. Kaul, A.K. Parhi, Y. Zhang, E.J. LaVoie, S. Tuske, E. Arnold, J.E. Kerrigan, D.S. Pilch, A
881 bactericidal guanidinomethyl biaryl that alters the dynamics of bacterial FtsZ polymerization, J.
882 Med. Chem. 55 (2012) 10160-10176.
883 [53] Q. Wang, L. Tan, K. Yang, Cytocompatibility and hemolysis of AZ31B magnesium alloy with
884 Si-containing coating, J. Mater. Sci. Technol. 31 (2015) 845-851.
885 [54] S. Wang, H. Wang, B. Ren, X. Li, L. Wang, H. Zhou, M.D. Weir, X. Zhou, R.M. Masri, T.W.
886 Oates, L. Cheng, H.H.K. Xu, Drug resistance of oral bacteria to new antibacterial dental monomer
887 dimethylaminohexadecyl methacrylate, Sci. Rep. 8 (2018) 1-11.
888 [55] J.K. Martin II, J.P. Sheehan, B.P. Bratton, G.M. Moore, A. Mateus, S.H.-J. Li, H. Kim, J.D.
889 Rabinowitz, A. Typas, M.M. Savitski, M.Z. Wilson, Z. Gitai, A dual-mechanism antibiotic kills
890 gram-negative bacteria and avoids drug resistance, Cell 181 (2020) 1518-1532.
891